JEM | Journal of Experimental Medicine

ARTICLE

Sox7 promotes high-grade glioma by increasing VEGFR2-mediated vascular abnormality

Il-Kug Kim[1]*, Kangsan Kim[1]*, Eunhyeong Lee[2], Dong Sun Oh[2], Chan Soon Park[1], Seongyeol Park[1], Jee Myung Yang[1], Ju-Hee Kim[1], Hyung-Seok Kim[3], David T. Shima[4], Jeong Hoon Kim[5], Seok Ho Hong[5], Young Hyun Cho[5], Young Hoon Kim[5], Jong Bae Park[6], Gou Young Koh[1,2,7], Young Seok Ju[1,2], Heung Kyu Lee[1,2], Seungjoo Lee[5], and Injune Kim[1,2]

High-grade glioma (HGG) is highly angiogenic, but antiangiogenic therapy has transient clinical benefit in only a fraction of patients. Vascular regulators of these heterogeneous responses remain undetermined. We found up-regulation of Sox7 and down-regulation of Sox17 in tumor endothelial cells (tECs) in mouse HGG. *Sox7* deletion suppressed VEGFR2 expression, vascular abnormality, hypoxia-driven invasion, regulatory T cell infiltration, and tumor growth. Conversely, *Sox17* deletion exacerbated these phenotypes by up-regulating Sox7 in tECs. Anti-VEGFR2 antibody treatment delayed tumor growth by normalizing *Sox17*-deficient abnormal vessels with high Sox7 levels but promoted it by regressing *Sox7*-deficient vessels, recapitulating variable therapeutic responses to antiangiogenic therapy in HGG patients. Our findings establish that Sox7 promotes tumor growth via vessel abnormalization, and its level determines the therapeutic outcome of VEGFR2 inhibition in HGG. In 189 HGG patients, Sox7 expression was heterogeneous in tumor vessels, and high Sox7 levels correlated with poor survival, early recurrence, and impaired vascular function, emphasizing the clinical relevance of Sox7 in HGG.

Introduction

Although vessel abnormality including tumor angiogenesis is a hallmark of cancer, its pattern and underlying mechanisms are various, depending on the tumor type (Hanahan and Weinberg, 2000, 2011; Carmeliet and Jain, 2011). High-grade glioma (HGG) is a cancer with prominent vessel abnormality (Jain et al., 2007; Takano, 2012; Das and Marsden, 2013). The molecules responsible for aberrant vessels have been elucidated, and their inhibition helps to reduce vessel abnormality in HGG animal models (Reis et al., 2012; Park et al., 2016). Although HGG is also characterized by angiogenic vessels, tumor angiogenesis is rarely observed in available HGG models; rather, tumor cells coopt preexisting vessels for growth (Blouw et al., 2003; Bergers and Hanahan, 2008; Takano, 2012). Because of difficulty in modeling, the molecular mechanisms of tumor angiogenesis in HGG remain elusive. How tumor angiogenesis is inactive in HGG models also remains unclear.

Tumor angiogenesis has been a target of cancer therapy. Though blockade of VEGF has been effective in treating several cancers (Saharinen et al., 2011), its clinical benefit is limited in HGG largely as a result of two different tumor behaviors: resistance and indifference. The resistance mechanisms to anti-VEGF (α-VEGF) therapy have been fairly elucidated: bevacizumab, an α-VEGF antibody (Ab), produces initial beneficial effects in a subpopulation of HGG patients, but tumors rapidly relapse via alternative angiogenic factors (Batchelor et al., 2007; Scholz et al., 2016) and enhanced tumor invasion (Pàez-Ribes et al., 2009; Lu et al., 2012). Because of this resistance, α-VEGF Ab failed to improve overall survival in HGG patients in large-scale clinical studies (Bergers and Hanahan, 2008; Chinot et al., 2014; Gilbert et al., 2014). However, regarding the presence or absence of beneficial outcome, HGG patients can be categorized into responder and nonresponder. The responders showed prolonged progression-free survival, and the nonresponders failed to show even transient therapeutic benefit (Chinot et al., 2014; Gilbert et al., 2014). Despite its limited clinical benefit, α-VEGF Ab is still used for treating HGG because there are few treatment options. How anti-VEGF therapy gives rise to different responses in HGG

patients remain to be determined to predict patients suitable for anti-VEGF therapies.

To understand the mechanism of the variable response to antiangiogenic therapy, we sought to identify angiogenic regulators in HGG. SoxF transcription factors consisting of Sox7, Sox17, and Sox18 are expressed specifically in endothelial cells (ECs) and contribute to vascular morphogenesis (Francois et al., 2010; Corada et al., 2013; Lee et al., 2014; Zhou et al., 2015). Sox7 and Sox17 genetically cooperate for developmental angiogenesis by reinforcing VEGF signaling (Kim et al., 2016). Although the role of Sox17 was found in subcutaneous ectopic tumors (Yang et al., 2013), Sox7 has not been studied in the context of tumor angiogenesis. In this study, we investigated the role of Sox7 and Sox17 in tumor angiogenesis in orthotopic mouse HGG models. In an HGG model, Sox7 promoted tumor angiogenesis, and Sox17 suppressed it. Sox7 levels in tumor vessels correlated with therapeutic efficacy of α-VEGFR2 Ab. In a large HGG patient population, Sox7 expression in tumor vessels was heterogeneous. High Sox7 levels correlated with poor prognosis and abnormal tumor vessels, emphasizing clinical relevance of Sox7 in HGG.

Results

Vascular characterization of murine HGG models

To reveal molecular mechanisms of vascular characteristics of HGG, we established a mouse orthotopic glioma model by intracranially injecting GL26l glioma cells into congenic B6 mice. GL261-derived glioma recapitulated the malignant characteristics of HGG (Fig. 1 A) as reported (Kerber et al., 2008). We studied the vascular features of GL261-derived HGG. Compared with nontumor brain vessels, HGG vessels exhibited twofold area, halved number (315/mm^2 of normal brain vs. 170/mm^2 of GL261 HGG), enlarged diameter, and halved branching (Fig. 1, B–E), implying that, rather than angiogenesis, regression and dilation are the major vascular changes in this tumor model. HGG vessels exhibited poor pericyte coverage, hyper-leakage, and hypoperfusion (Fig. 1, F–H). Thus, orthotopic GL261 HGG is characterized by aberrant vasodilation and impaired vascular function.

To identify the molecular players for vessel abnormality, we profiled the endothelial transcriptomics of HGG and brain. Two endothelial populations expressed a total 15,111 genes, and 346 genes were differentially expressed by more than twofold (Fig. 1 I). Suppressed Wnt signaling was predicted in tumor ECs (tECs; Fig. 1 J) in line with dysregulated endothelial Wnt signaling in brain tumors (Reis et al., 2012; Phoenix et al., 2016). Gene ontology analysis showed the greatest changes in the category of transcriptional regulation (Fig. 1 K). Notably, angiogenic transcription factor Sox7 was up-regulated in tECs (Fig. 1 L), suggesting its role in vessel abnormality in HGG. We examined Sox7 expression in low-grade glioma and HGG patients. Nontumor human brain vessels had no detectable Sox7 expression (Fig. 1 M). Although vascular expression of Sox7 was detected in a fraction of grade II glioma tissues, its frequency and intensity were higher in grade III/IV glioma tissues (Fig. 1, N–O), suggesting clinical relevance of Sox7 expression in HGG.

Opposing expression patterns of Sox7 and Sox17 in HGG vessels

We verified vascular Sox7 expression in orthotopic GL261 HGG grown in Sox7$^{mCh/+}$ mice. Consistent with the RNA sequencing data, 63% of HGG vessels expressed Sox7-mCherry fluorescence, whereas nontumor brain vessels rarely expressed it (Fig. 2 A). Because Sox17 is homologous to Sox7 in DNA sequence, we examined vascular Sox17 expression in GL261 HGG grown in Sox17$^{GFP/+}$ mice. 41% of nontumor brain vessels, but only 15% of HGG vessels, expressed Sox17-GFP fluorescence (Fig. 2 B). Robust Sox7 expression and decreased Sox17 expression were confirmed in HGG vessels from wild-type mice (Fig. S1, A and B) and a patient-derived xenograft HGG model (Fig. S1, C and D; Yin et al., 2017). In confocal microscopy, 48% of tECs (149 out of 308) exhibited Sox7 immunostaining in their nuclei, whereas none of ~40 pericytes exhibited Sox7 immunostaining, indicating that Sox7 is specifically expressed in the tECs of HGG vessels (Fig. S1 E). These results reveal different endothelial expression patterns for Sox7 and Sox17 in HGG and nontumor brain.

In contrast, Sox17 was previously shown to be highly expressed in tumor vessels in a subcutaneous ectopic Lewis lung carcinoma (LLC) model (Yang et al., 2013). To clarify the cause of different Sox17 expression patterns between these tumor models, we examined Sox7 and Sox17 expression in tumor vessels by injecting GL261 or LLC cells into Sox7$^{mCh/+}$ and Sox17$^{GFP/+}$ mice either intracranially or subcutaneously. In GL261- and LLC-derived tumors grown in brain, >60% of tumor vessels expressed Sox7-mCherry, but only 12–15% of them expressed Sox17-GFP (Fig. 2, C and E). However, in GL261- and LLC-derived tumors grown subcutaneously, 75–80% of tumor vessels expressed both Sox7-mCherry and Sox17-GFP (Fig. 2, D and E). In contrast, embryonic and neonatal brain vessels featured by angiogenic tip cells robustly expressed both Sox7 and Sox17 (Fig. 2 F). These results demonstrate that the expression pattern of Sox7 and Sox17 in HGG vessels is controlled by the growth environment in the brain rather than the identity of tumor cells and suggest that this brain-specific regulation in tumor vessels differs from regulation in developing brain vessels.

Given the contrasting vascular expression of Sox7 and Sox17 in HGG, we examined their expression in individual tumor vessels. Sox7 immunostaining was evident in Sox17-GFP–low vessels but decreased in Sox17-GFP–high vessels (Fig. 2 G). Sox17 immunostaining was rare in Sox7-mCherry–high vessels but prominent in Sox7-mCherry–low vessels (Fig. 2 H). These findings indicate an inverse relationship between Sox7 and Sox17 expression in HGG vessels. Likewise, no coincident vascular expression of Sox7 and Sox17 was observed in grade III/IV glioma tissues (Fig. 2 I). Compared with Sox7-mCherry–low or Sox17-GFP–high tumor vessels, Sox7-mCherry–high or Sox17-GFP–low tumor vessels had twofold tortuosity, twofold branching, and moderately narrow diameters (Fig. S1, F and G). Similarly, Sox7-positive tumor vessels had more tortuosity and branching and narrow diameters relative to Sox17-positive tumor vessels in GL261 HGG grown in wild-type mice, patient-derived xenograft HGG, and grade III/IV patient glioma samples (Fig. S1, I and J). The expression pattern of Sox7 and Sox17 being associated with contrasting vascular morphology
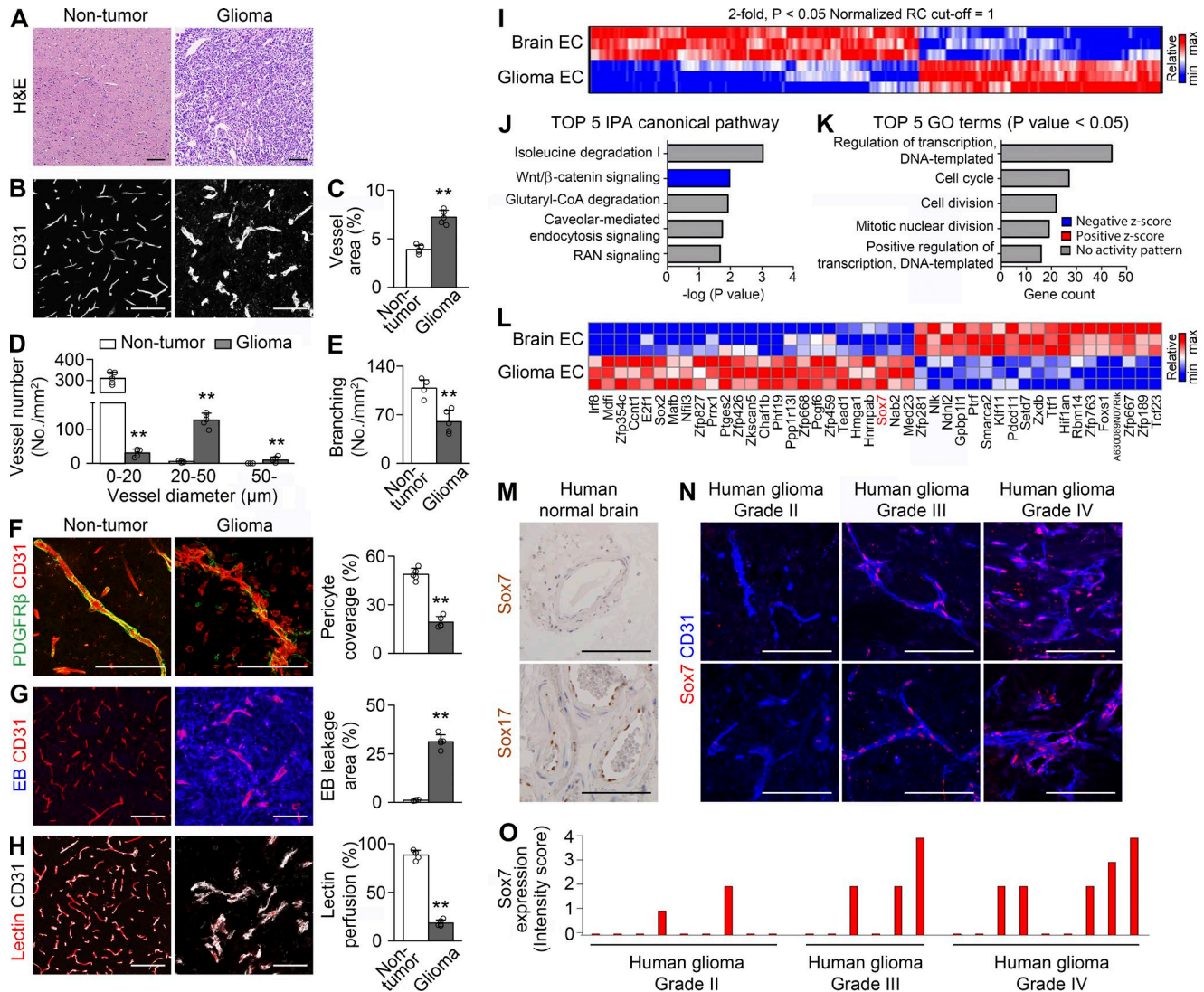
Figure 1. **Abnormal vessels in HGG have distinct endothelial transcripts. (A–H)** H&E staining (A) and CD31-positive vessels (B–H) in nontumor brain and orthotopic HGG. (B–E) Vascular network (B) and quantification of vessel area (C), vessel number based on vessel diameter (D), and vessel branching (E). (F) PDGFRβ-positive pericytes and quantification of coverage. (G) Evans blue (EB) and quantification of extravasation. (H) Lectin and quantification of vascular perfusion. Values are presented as mean ± SD ($n = 5$). **, P < 0.01. **(I–L)** Transcriptome analyses of normal brain and HGG ECs by RNA sequencing ($n = 3$). (I–K) Heat map (I), top five canonical pathways by the ingenuity pathway analysis (IPA; J), and top five gene ontology (GO) terms in biological processes (K) using 346 genes differentially expressed by more than twofold (P < 0.05). (L) Heat map of differentially expressed genes in the category of transcriptional regulation. **(M)** No Sox7 but robust Sox17 immunostaining in human nontumor brain vessels. **(N and O)** Sox7 immunostaining in tumor vessels from glioma patients with different grades (N) and intensity scores of nine grade II, six grade III, and nine grade IV patients (O) Bars, 100 µm.

suggests that Sox7 and Sox17 may regulate vascular morphogenesis in an opposing manner in HGG.

We examined Sox7 and Sox17 expression in various tissues. Sox17, but not Sox7, was expressed in retina capillaries as in brain capillaries (Fig. S1 K), but Sox7 and Sox17 showed coincidental expression in the capillaries of gastrointestinal tissues and arteries of the skin (Fig. S1, L–N). Thus, the pattern of Sox7 and Sox17 expression is contextually heterogeneous in adult vessels.

Sox7 deletion delays HGG growth by attenuating vascular abnormality

To reveal the role of Sox7 in HGG vessels, we studied tumor progression and tumor vessels by excising floxed *Sox7* alleles from the ECs of mutant mice, *Cdh5*-CreER^T2;*Sox7*^fl/fl (*Sox7*^iΔEC),

bearing orthotopic HGG derived from GFP-expressing GL261. Sox7 expression was not detectable after tamoxifen administration (Fig. S2 A). Mutant mice lacking endothelial *Sox7* had decreased tumor size 3 wk after implantation (Fig. 3 A), and their survival extended (median survival: 33 d in *Sox7*^iΔEC mice vs. 28 d in controls; Fig. 3 B).

We studied the morphology of *Sox7*-deficient HGG vessels. As mentioned earlier in this paper, HGG vessels in wild-type mice had a decreased number and branching, but substantial increase in diameter, thereby leading to twofold increased vessel area relative to nontumor brain vessels (Fig. 1, B–E). Compared with changes in control HGG vessels, *Sox7*-deficient vessels had less of a decline in number, more severe decrease in branching, and a modest increase in diameter, resulting in no significant increase
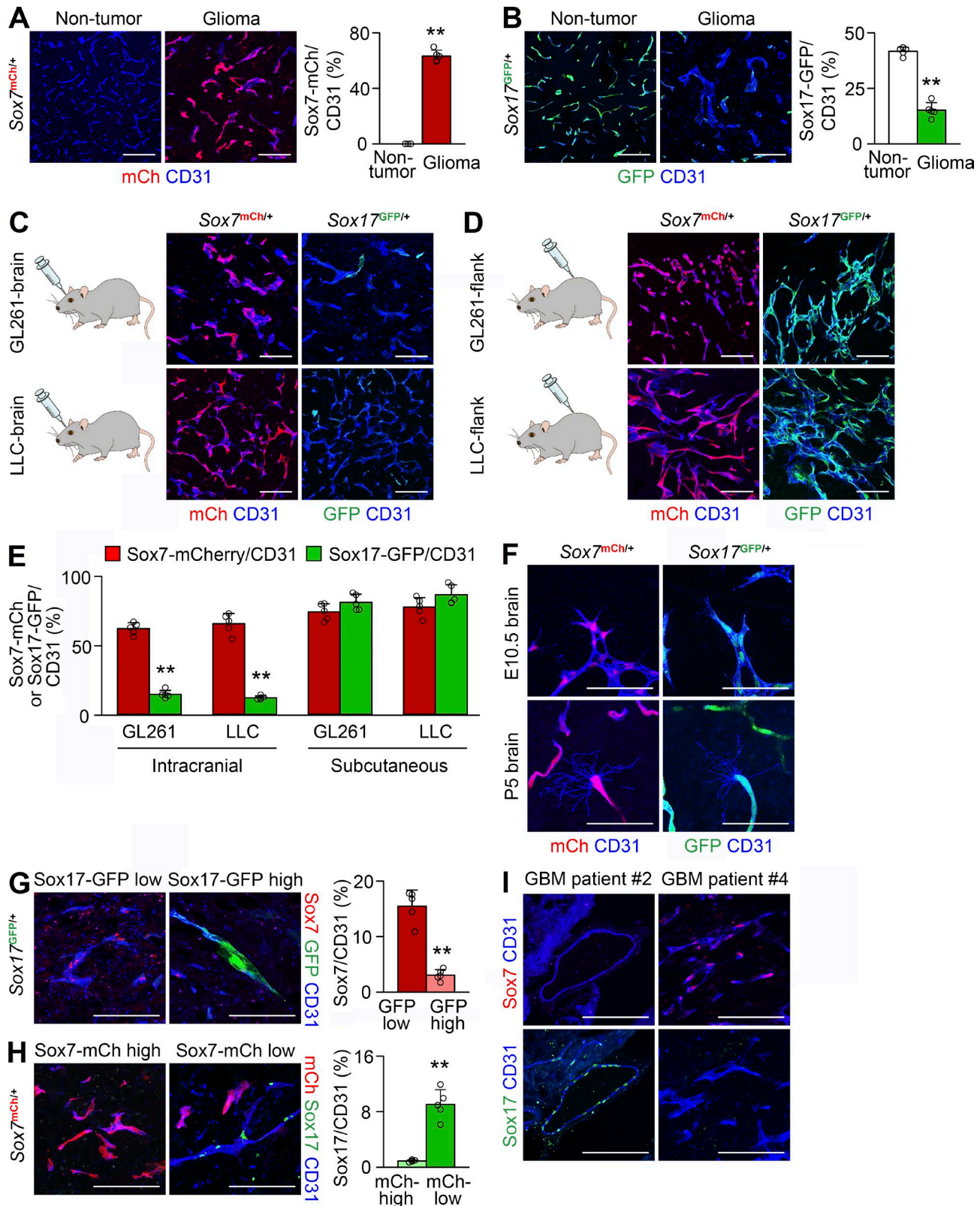
Figure 2. **Sox7 is up-regulated in HGG vessels. (A–H)** CD31-positive vessels in $Sox7^{mCh/+}$ and $Sox17^{GFP/+}$ mice. (A and B) Sox7-mCherry (A) and Sox17-GFP (B) fluorescence and signal quantification in nontumor brain and tumor vessels of mice bearing orthotopic GL261 HGG. (C and D) Sox7-mCherry and Sox17-GFP fluorescence in tumor vessels. GL261- and LLC-derived intracranial (C) and subcutaneous tumors (D). (E) Quantification of fluorescence signals in C and D. (F) Robust Sox7-mCherry and Sox17-GFP signals in brain vessels on embryonic day 10.5 (E10.5) and postnatal day 5 (P5). (G) Sox7 immunostaining and its quantification in Sox17-GFP–low and –high vessels in GL261 HGG. (H) Sox17 immunostaining and its quantification in Sox7-mCherry–high and –low vessels in GL261 HGG. **(I)** Sox7 and Sox17 immunostaining in tumor vessels using adjacent sections from the same HGG patients. Values are presented as mean ± SD (n = 5). **, P < 0.01. Bars: 100 µm (A–D and G–I); 50 µm (F).
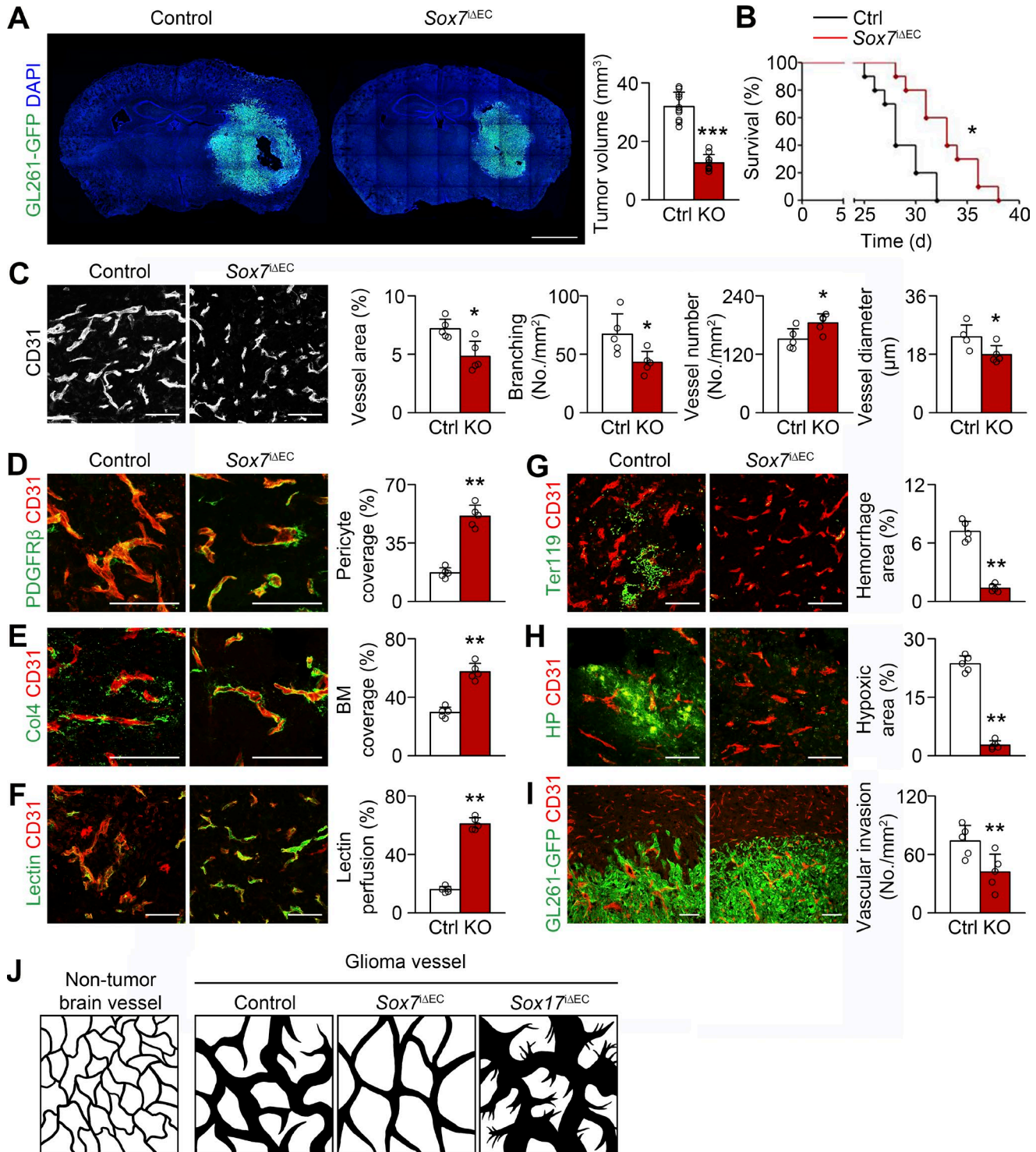
Figure 3. **Sox7 deletion delays HGG growth by reducing vessel abnormality. (A)** GL261-GFP HGGs grown in control (Ctrl) and $Sox7^{i\Delta EC}$ (KO) mice and quantification of tumor volume (n = 10). **(B)** Survival curves for HGG-bearing mice (n = 10). *, P < 0.05 (log-rank test). **(C-I)** CD31-positive HGG vessels in control and KO mice. (C) Normalized vessel morphology by $Sox7$ deletion and quantification of vessel area, branching, number, and diameter. (D and E) PDGFRβ-positive pericytes (D) and Col4-positive basement membrane (BM; E) and quantification of coverage. (F) Lectin and quantification of vascular perfusion. (G) Ter119-positive erythrocytes and quantification of hemorrhage. (H) Pimonidazole adduct (hypoxyprobe, HP) and quantification of hypoxic area. (I) Reduced perivascular invasion of GL261-GFP tumor cells by $Sox7$ deletion. **(J)** Diagrams depicting normal brain vessels and control, $Sox7$-deficient, and $Sox17$-deficient HGG vessels. Values are presented as mean ± SD (n = 5 unless otherwise denoted). *, P < 0.05; **, P < 0.01; ***, P < 0.001. Bars: 2 mm (A); 100 μm (C–I).
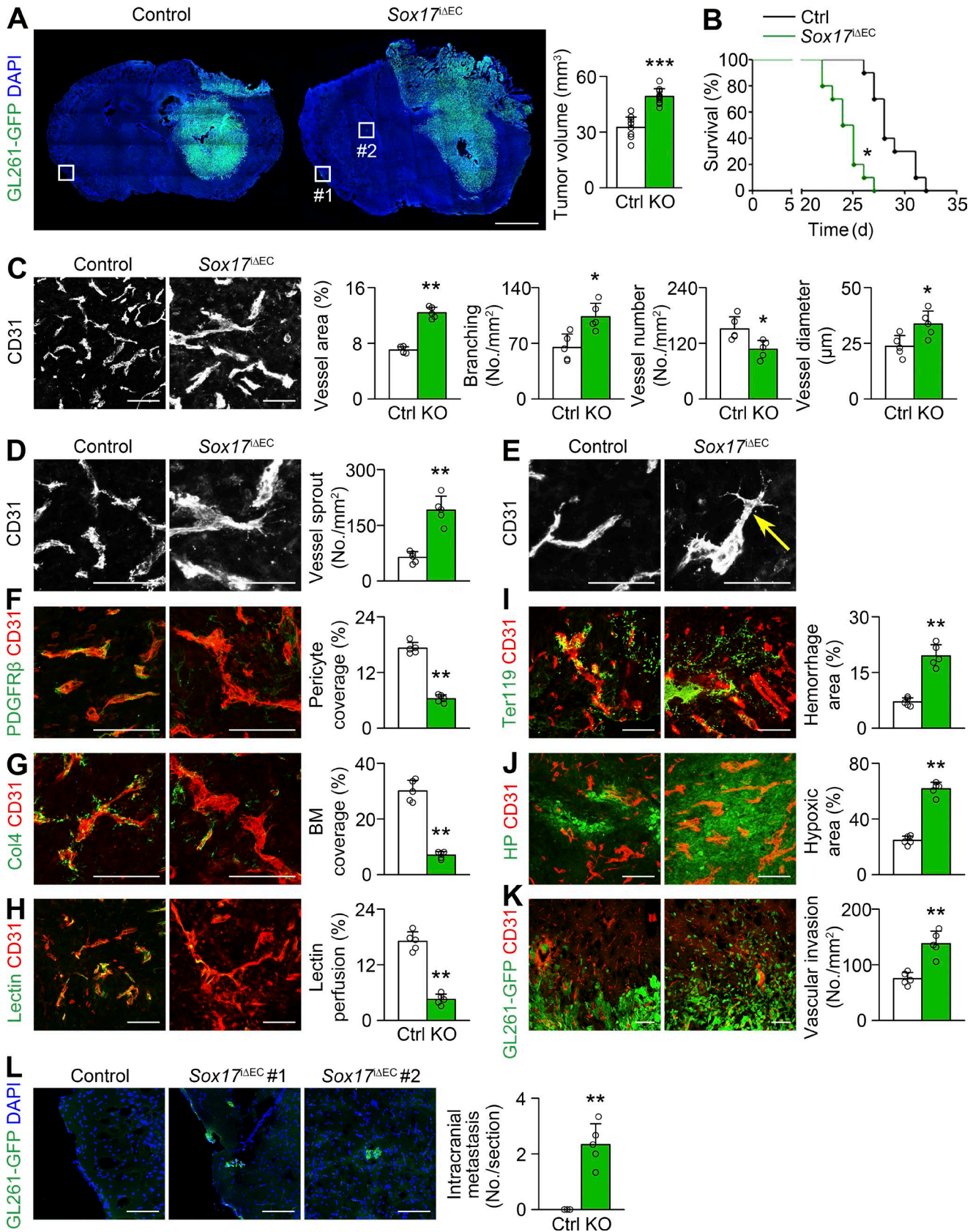
Figure 4. **Sox17 deletion promotes HGG growth by increasing vessel abnormality. (A)** GL261-GFP HGGs grown in control (Ctrl) and *Sox17*$^{\Delta EC}$ (KO) mice and quantification of tumor volume (*n* = 10). **(B)** Survival curves for HGG-bearing mice (*n* = 10). *, P < 0.05 (log-rank test). **(C–K)** CD31-positive HGG vessels in control and KO mice. (C) Increased vessel abnormality with *Sox17* deletion and quantification of vessel area, branching, number, and diameter. (D and E) Increased sprouting (D) and appearance of tip cells (arrow) by *Sox17* deletion (E). (F and G) PDGFRβ-positive pericytes (F) and Col4-positive basement membrane

in vessel area compared with nontumor brain vessels (Fig. 3, C and J). Pericytes, basement membrane, and junctional VE-cadherin were restored in *Sox7*-deficient vessels relative to control HGG vessels (Fig. 3, D–E; and Fig. S2 B). Increased perfusion, decreased leakage, and reduced microhemorrhage were found in *Sox7*-deficient vessels (Fig. 3, F and G; and Fig. S2 C). In line with this, *Sox7* deletion substantially diminished tumor hypoxia (Fig. 3 H). However, *Sox7* deletion induced no discernable vessel changes in nontumor brain tissues (Fig. S3, A–F). These results indicate that *Sox7* deletion can rescue the morphology, structure, and function of the HGG vascular network.

We explored how *Sox7* deletion suppresses tumor growth by examining cellular changes in tumor tissues. *Sox7* ablation reduced necrosis, apoptosis, and proliferation, which is unlikely to explain tumor growth suppression (Fig. S2, D–F). Hypoxia is known to trigger tumor invasion. *Sox7* ablation inhibited tumor invasion at the border (Fig. 3 I and Fig. S2 G). These results suggest decreased tumor invasion by the relief of hypoxic stress as a cellular mechanism for delayed tumor growth by *Sox7* deletion.

Sox17 deletion promotes HGG growth by exacerbating vascular abnormality

Given the association of Sox17 expression with particular vessel morphology, we studied the role of Sox17 in tumor progression and tumor vessels by deleting endothelial *Sox17* alleles from mutant mice, *Cdh5*-CreER^{T2};*Sox17*$^{fl/fl}$ (*Sox17*^{iΔEC}), bearing orthotopic GL261-GFP HGG. Effective *Sox17* deletion was confirmed by a lack of Sox17 immunostaining in brain arteries (Fig. S2 H). Compared with controls, mutant mice lacking endothelial *Sox17* showed increased tumor growth 3 wk after implantation (Fig. 4 A) and succumbed to tumor burden earlier (median survival: 24.5 d in *Sox17*^{iΔEC} mice vs. 28 d in controls; Fig. 4 B).

Regarding vessel morphology, *Sox17*-deficient HGG vessels exhibited a greater decrease in number but greater increase in branching and diameter than control HGG vessels, leading to a further 1.8-fold increase in vascular area (Figs. 3 J and 4 C). Interestingly, in contrast to control and *Sox7*-deficient HGG vessels, *Sox17*-deficient HGG vessels had abundant sprouts (Fig. 4 D) and tip cells, a morphological hallmark of sprouting angiogenesis (Fig. 4 E). *Sox17*-deficient vessels exhibited a more severe deficiency of pericytes, basement membrane, and junctional VE-cadherin than control HGG vessels (Fig. 4, F and G; and Fig. S2 I). The severity of hypoperfusion, leakage, and microhemorrhage was increased in *Sox17*-deficient vessels compared with control HGG vessels (Fig. 4, H and I; and Fig. S2 J). Concomitantly, *Sox17* deletion increased tumor hypoxia (Fig. 4 J). In contrast, *Sox17* deletion induced no noticeable vessel changes in nontumor brain tissues (Fig. S3, H–M). These findings indicate that *Sox17* deletion can promote tumor angiogenesis and aggravate morphological, structural, and functional abnormalities of HGG vessels. Notably,

Sox17 deletion affected tumor progression, tumor vessels, and the oxygen environment in an opposite manner to *Sox7* deletion.

We studied mechanisms of promoted tumor growth by *Sox17* deletion. *Sox17* deletion promoted necrosis, apoptosis, and proliferation (Fig. S2, K–M), which is unlikely to underlie accelerated tumor growth. However, *Sox17* deletion increased tumor infiltration into surrounding brain tissue (Fig. 4 K and Fig. S2 N). In addition, intracranial metastasis was observed in mutant mice lacking endothelial *Sox17*, compared with no metastasis in controls (Fig. 4 L). These results suggest that *Sox17* deletion exacerbates hypoxia-driven tumor invasion, thereby promoting tumor growth.

Sox7 is up-regulated in HGG vessels via Dll4-induced Sox17 down-regulation

Sox7 and Sox17 are opposing regulators and inversely expressed in HGG. We studied whether Sox7 and Sox17 can suppress the expression of one another in HGG vessels. *Sox17*-deficient vessels expressed Sox7 more abundantly (1.5-fold) than control HGG vessels (Fig. 5 A). *Sox7*-deficient vessels expressed Sox17 at a comparable level with control HGG vessels (Fig. 5 B). However, *Sox7* or *Sox17* deletion resulted in no discernable changes in Sox17 and Sox7 expression in nontumor brain vessels (Fig. S3, G and N). These findings indicate that Sox17 can inhibit Sox7 expression, but Sox7 does not repress Sox17 expression in HGG vessels.

We further studied whether increased Sox7 expression in *Sox17*-deficient HGG vessels is functionally important. Phenotypes severely abnormal for tumor growth (Fig. 5 C), tumor vessels (Fig. 5, D–H), and tumor hypoxia (Fig. 5 I) caused by *Sox17* deletion were significantly rescued by additional *Sox7* deletion as shown by the attenuated abnormalities in mutant mice lacking both *Sox7* and *Sox17*, suggesting Sox7 up-regulation as one of the mechanisms of tumor and vessel abnormalities enhanced by *Sox17* deletion. These results also suggest a correlation in the level of Sox7 expression with the severity of HGG and HGG vessels.

Dll4 signaling inhibited Sox17 expression in tumor vessels in our previous study of a subcutaneous LLC tumor model (Lee et al., 2014). In contrast to the lack of detectable expression in normal brain vessels, Dll4 expression was substantial in HGG vessels, but it was merely modest in other cells (Fig. 6 A). We explored whether Dll4 signaling can down-regulate Sox17 in HGG vessels by excising endothelial *Dll4*. *Dll4* deletion reduced tumor growth and affected HGG vessels, as shown by decreased vessel area and diameter (Fig. 6, B–E). *Dll4*-deficient HGG vessels expressed Sox17 at fourfold higher levels than control HGG vessels, but Sox7 was expressed at one-fourth the level of control HGG vessels (Fig. 6, F and G). We elucidated whether repressed Sox7 expression by *Dll4* deletion was mediated by increased Sox17 expression. α-Dll4 neutralizing Ab repressed Sox7 expression in control HGG vessels similar to genetic *Dll4* ablation, but not in *Sox17*-deficient vessels (Fig. 6 H), indicating the need for Sox17

(BM; G) and quantification of coverage. (H) Lectin and quantification of vascular perfusion. (I) Ter119-positive erythrocytes and quantification of hemorrhage. (J) Hypoxyprobe (HP) adduct and quantification of hypoxic area. (K) Enhanced perivascular invasion of GL261-GFP tumor cells by *Sox17* deletion. **(L)** Enlarged images of boxed area in A showing intracranial metastasis in KO mice and its quantification. Values are presented as mean ± SD (n = 5 unless otherwise denoted). *, P < 0.05; **, P < 0.01; ***, P < 0.001. Bars: 2 mm (A); 50 μm (E); 100 μm (C, D, and F–L).
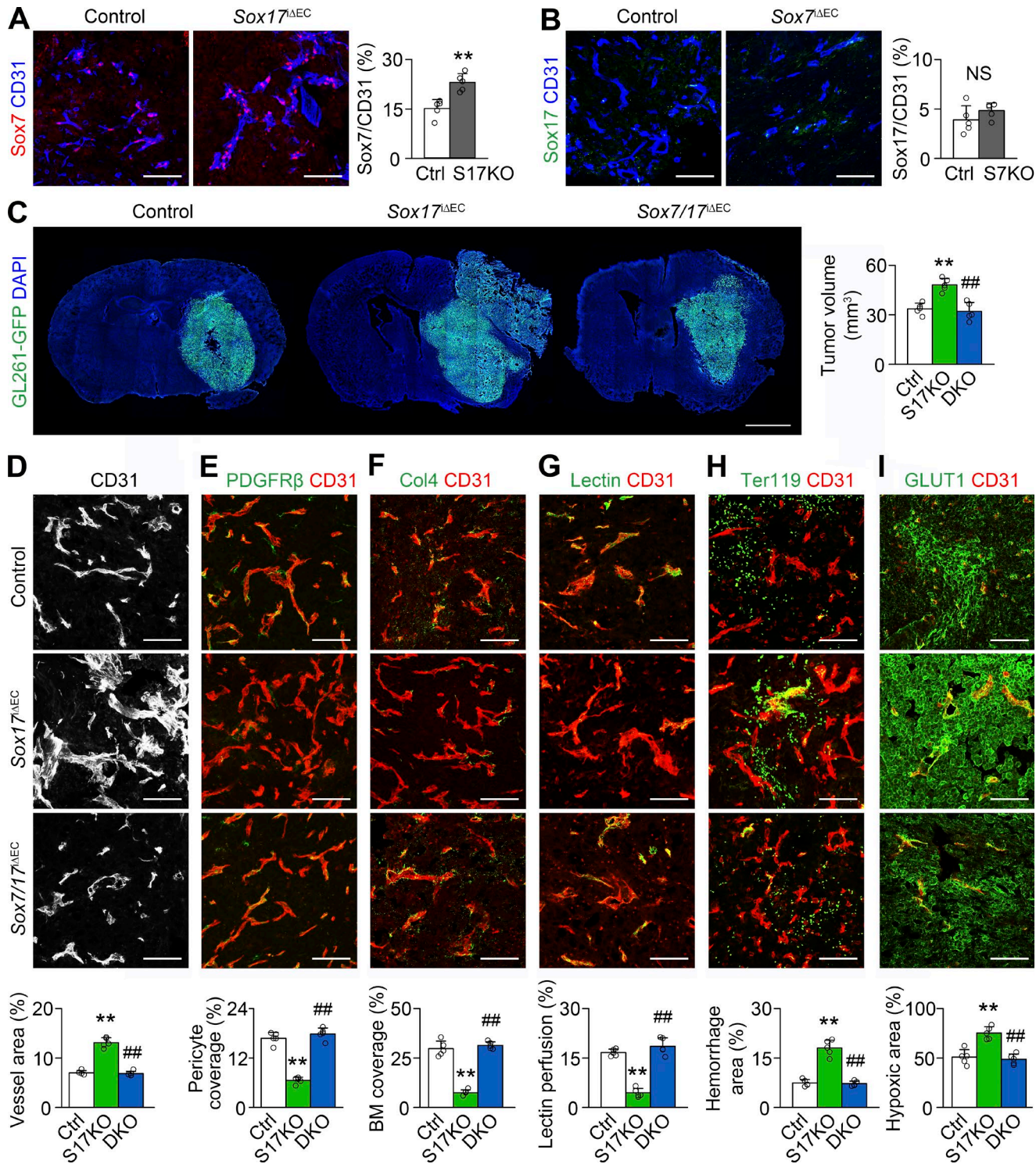
Figure 5. Sox7 up-regulation is responsible for further vascular abnormality in *Sox17*-deficient HGG vessels. (A and B) Sox7 (A) and Sox17 (B) immunostaining and quantification in HGG vessels of control, *Sox7*^ΔEC^ (S7KO), or *Sox17*^ΔEC^ (S17KO) mice. **(C)** GL261-GFP HGGs grown in control, S17KO, and *Sox7/17*^ΔEC^ (DKO) mice and quantification of tumor volume (*n* = 10). **(D–I)** CD31-positive HGG vessels in control, S17KO, and DKO mice. (D) Vascular network and quantification of vessel area. (E and F) PDGFRβ-positive pericytes (E) and Col4-positive basement membrane (BM; F) and quantification of coverage. (G) Lectin and quantification of vascular perfusion. (H) Ter119-positive erythrocytes and quantification of hemorrhage. (I) GLUT1 immunostaining and quantification of hypoxic area. Values are presented as mean ± SD (*n* = 5 unless otherwise denoted). **, P < 0.01 versus control; ##, P < 0.01 versus *Sox17*^ΔEC^. NS, not significant. Bars: 100 µm (A, B, and D–I); 2 mm (C).

in Sox7 repression. α-Dll4 Ab increased Sox17 expression in both control and *Sox7*-deficient HGG vessels (Fig. 6 I), indicating the independence of Sox17 up-regulation from Sox7. These results

suggest a regulatory axis in which Dll4 is turned on in HGG vessels, repressing Sox17 expression and subsequently up-regulating Sox7, which is crucial for tumor vessel abnormalization.

Because a previous study identified Sox17 as a stimulator of Dll4 expression in arterial differentiation (Corada et al., 2013), we examined Dll4 expression in *Sox7*- and *Sox17*-deficient HGG vessels. Dll4 was not changed in *Sox7*-deficient vessels but was increased in *Sox17*-deficient vessels (Fig. 6 J), suggesting that, unlike arterial differentiation, Sox7 and Sox17 are not upstream of Dll4 in HGG. Increased hypoxia by *Sox17* deletion may enhance Dll4 expression in tumor vessels (Patel et al., 2005).

VEGFR2 inhibition induces a variable tumor response based on Sox7 levels in tumor vessels
To understand the molecular characteristics of *Sox7*- and *Sox17*-deficient tECs, we correlated their gene expression profiles. Between *Sox7*-deficient and control tECs, 2,165 genes were differentially expressed using twofold criteria, including down-regulation of *Sox7* transcripts (log$_2$fold change = –5.28). Gene set enrichment analysis using the GSEA tool with 2,165 genes identified four gene sets with significant differences: angiogenesis and Wnt–β-catenin pathway (both enriched in control tECs) and DNA repair and allograft rejection (both enriched in *Sox7*-deficient tECs; Fig. 7 A). These data suggest that *Sox7*-deficient tECs are less angiogenic, more resistant to DNA damage stress, and more greatly associated with T cell–mediated immunity. Between *Sox17*-deficient and control tECs, 1,756 genes were differentially expressed, including down-regulation of *Sox17* transcripts (log$_2$fold change = –7.25). Significant differences were identified in glycolysis and cell cycle progression signature gene sets, including MYC targets, E2F targets, and G2M checkpoint (Fig. 7 B), suggesting altered cellular metabolism and proliferating capacity in *Sox17*-deficient tECs.

Given the fundamental role of VEGF signaling in tumor vessels, we examined VEGFR2 expression in *Sox7*- and *Sox17*-deficient HGG vessels. Compared with controls, VEGFR2 expression was repressed in *Sox7*-deficient vessels but was up-regulated in *Sox17*-deficient vessels (Fig. 7, C and D), indicating that Sox7 promotes and Sox17 represses VEGFR2 expression in HGG vessels. In addition, *Sox17*-deficient vessels showed increased levels of phosphor-VEGFR2 (at Tyr1175), phosphor-ERK (at Thr202 and Tyr204 of ERK1 and Thr185 and Tyr187 of ERK2), and phosphor-Akt (at Ser473), reflecting functionally activated VEGFR2 signaling by *Sox17* deletion (Fig. 7, E–G).

To determine whether VEGFR2 up-regulation is responsible for increased vessel abnormality, we administered DC101, α-VEGFR2 blocking Ab, or control Ab to *Sox17*$^{i\Delta EC}$ mice bearing orthotopic HGG. Compared with control Ab, DC101 administration decreased tumor size to the size of tumors grown in control mice (Fig. 8, A and G) and significantly extended the survival of HGG-bearing *Sox17*$^{i\Delta EC}$ mice (median survival: 28 d on DC101 treatment vs. 24 d on control Ab; Fig. 8 H). DC101, but not control Ab, attenuated the abnormality of *Sox17*-deficient vessels by decreasing vascular area and sprouts (Fig. 8, B, I, and J) and restoring basement membrane to the extent of control HGG vessels (Fig. 8, C and K). DC101 also diminished microhemorrhage, hypoxia, and invasion within tumors grown in *Sox17*$^{i\Delta EC}$ mice to the level of tumors grown in control mice (Fig. 8, D–F and L–N). These results suggest that VEGFR2 up-regulation is a

key mechanism underlying overall adverse changes induced by *Sox17* deletion.

We examined the effect of VEGFR2 inhibition in control mice with moderate VEGFR2 expression in HGG vessels. Compared with control Ab, DC101 suppressed tumor growth (Fig. 8, A and G) and induced a modest survival benefit (median survival: 29.5 d on DC101 treatment vs. 27.5 d on control Ab; Fig. 8 H). DC101 also suppressed area, sprouts, and basement membrane coverage of control HGG vessels compared with control Ab (Fig. 8, B, C, and I–K), featuring vessel regression. In line with this, DC101 increased hypoxia and invasion within tumors grown in control mice (Fig. 8, E, F, M, and N). Phenotypes induced by VEGFR2 inhibition in control mice were consistent with a previous study (Pàez-Ribes et al., 2009) showing that VEGF signaling blockade inhibits tumor growth transiently but triggers a resistant response to severe hypoxia.

Because VEGFR2 expression was remarkably lower in *Sox7*-deficient vessels compared with control HGG vessels, we studied whether VEGFR2 blockade is also able to inhibit tumor growth in *Sox7*$^{i\Delta EC}$ mice. In contrast to control and *Sox17*$^{i\Delta EC}$ mice, DC101 increased tumor growth in *Sox7*$^{i\Delta EC}$ mice (Fig. 8, A and G) and shortened the survival of HGG-bearing *Sox7*$^{i\Delta EC}$ mice (median survival: 31.5 d on DC101 treatment vs. 33.5 d on control Ab; Fig. 8 H). DC101 decreased the area and basement membrane in *Sox7*-deicient vessels (Fig. 8, B, C, and I–K). DC101 aggravated microhemorrhage and hypoxia in tumor tissues and promoted tumor invasion in *Sox7*$^{i\Delta EC}$ mice (Fig. 8, D–F and L–N). These findings indicate that VEGFR2 inhibition can adversely affect tumor progression by inducing severe vascular rarefaction in the *Sox7*-deficient context and suggest that low levels of Sox7 and VEGFR2 may be associated with poor outcomes after VEGFR2 blockade in the treatment of HGG.

Sox7 deletion inhibits HGG by boosting T cell–mediated tumor immunity
Because impaired T cell immunity is central to immune suppression in cancers, we assessed the abundance of CD4$^+$ helper T cells, CD8$^+$ cytotoxic T cells, and FoxP3$^+$ regulatory T cells (T reg cells) in HGG grown in *Sox7*$^{i\Delta EC}$ and *Sox17*$^{i\Delta EC}$ mice. Compared with control, *Sox7* deletion increased CD8$^+$ T cells and decreased T reg cells, whereas *Sox17* deletion increased T reg cells (Fig. 9, A–D). The frequency of CD4$^+$ T cells was not changed (Fig. 9, A and B). In contrast to HGG, T reg cells were very rare in normal brain tissue (Fig. 9 E). Considering that T reg cells suppress the cytotoxic function of CD8$^+$ T cells (Nishikawa and Sakaguchi, 2014), these findings suggest that *Sox7* deletion enhances T cell–mediated immunity, but *Sox17* deletion inhibits it by regulating T reg cell abundance specifically in HGG tissues.

To understand the underlying mechanisms, we measured the tumoral concentration of CCL17, CCL22, and CCL5, well-known chemokines for T reg cell recruitment (Curiel et al., 2004; Mizukami et al., 2008; Schlecker et al., 2012). *Sox7* deletion reduced the concentration of CCL17, CCL22, and CCL5, whereas *Sox17* deletion increased the CCL17 concentration (Fig. 9 F). These results suggest that Sox7 and Sox17 regulate CCL5/17/22-mediated T reg cell recruitment into tumor tissues, leading to immune control of HGG growth.
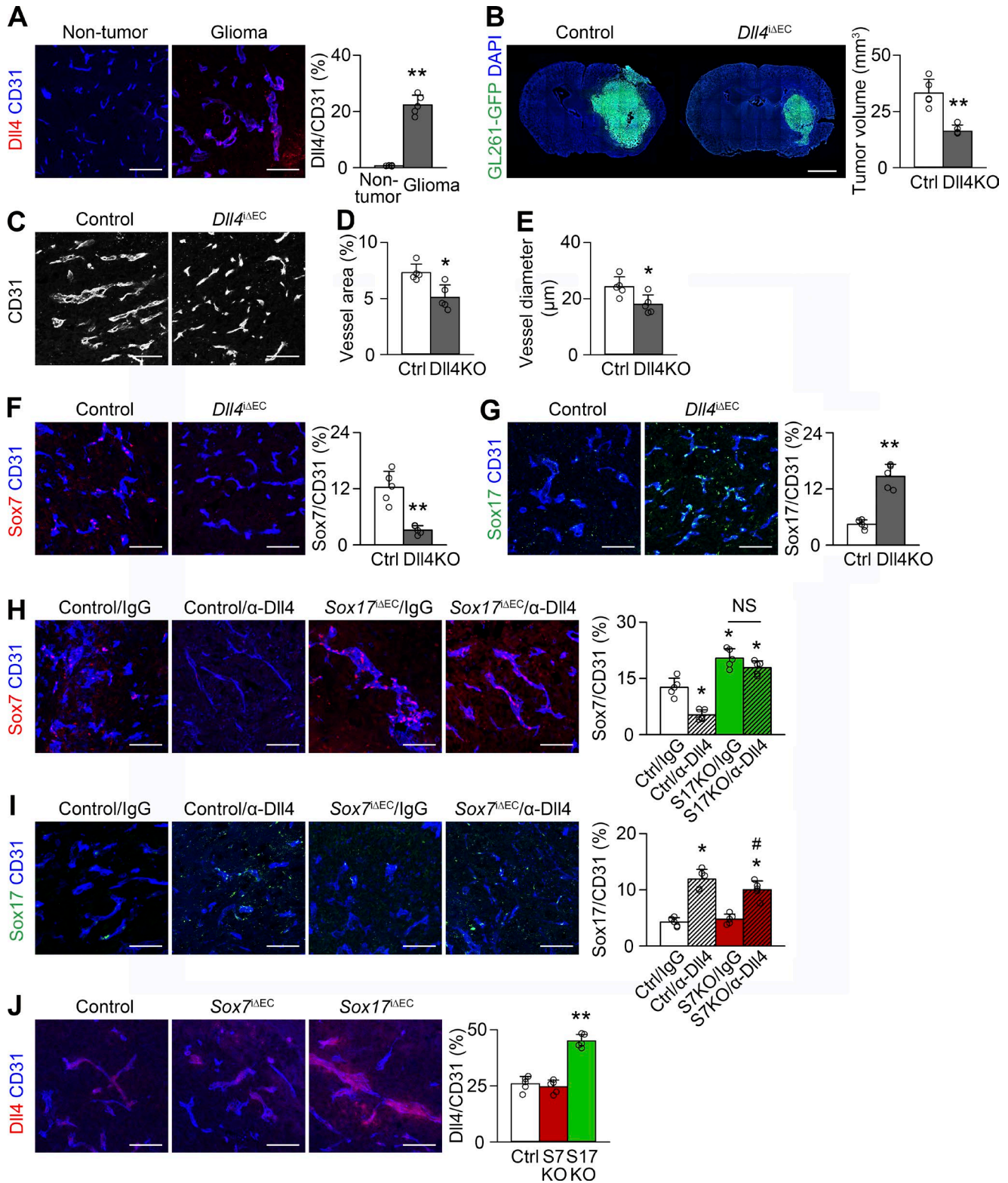
Figure 6.   **Dll4 increases Sox7 expression in HGG vessels via Sox17 down-regulation. (A)** Dll4 immunostaining in nontumor brain and HGG vessels. **(B)** GL261-GFP HGGs grown in control (Ctrl) and *Dll4*[iΔEC] (Dll4KO) mice and quantification of tumor volume. **(C-E)** CD31-positive HGG vessels in control and Dll4KO mice (C) and quantification of vessel area (D) and diameter (E). **(F and G)** Sox7 (F) and Sox17 (G) immunostaining and quantification in HGG vessels of control and Dll4KO mice. **(H and I)** Sox7 (H) and Sox17 (I) immunostaining and quantification in HGG vessels of control, *Sox7*[ΔEC] (S7KO), or *Sox17*[ΔEC] (S17KO) mice administered control (IgG) or α-Dll4 Ab. **(J)** Dll4 immunostaining and quantification in HGG vessels from control, *Sox7*[ΔEC], and *Sox17*[ΔEC] mice. Values are presented as mean ± SD (*n* = 5). *, P < 0.05; **, P < 0.01 versus control; #, P < 0.05 versus *Sox17*[ΔEC]. NS, not significant. Bars, 100 μm.
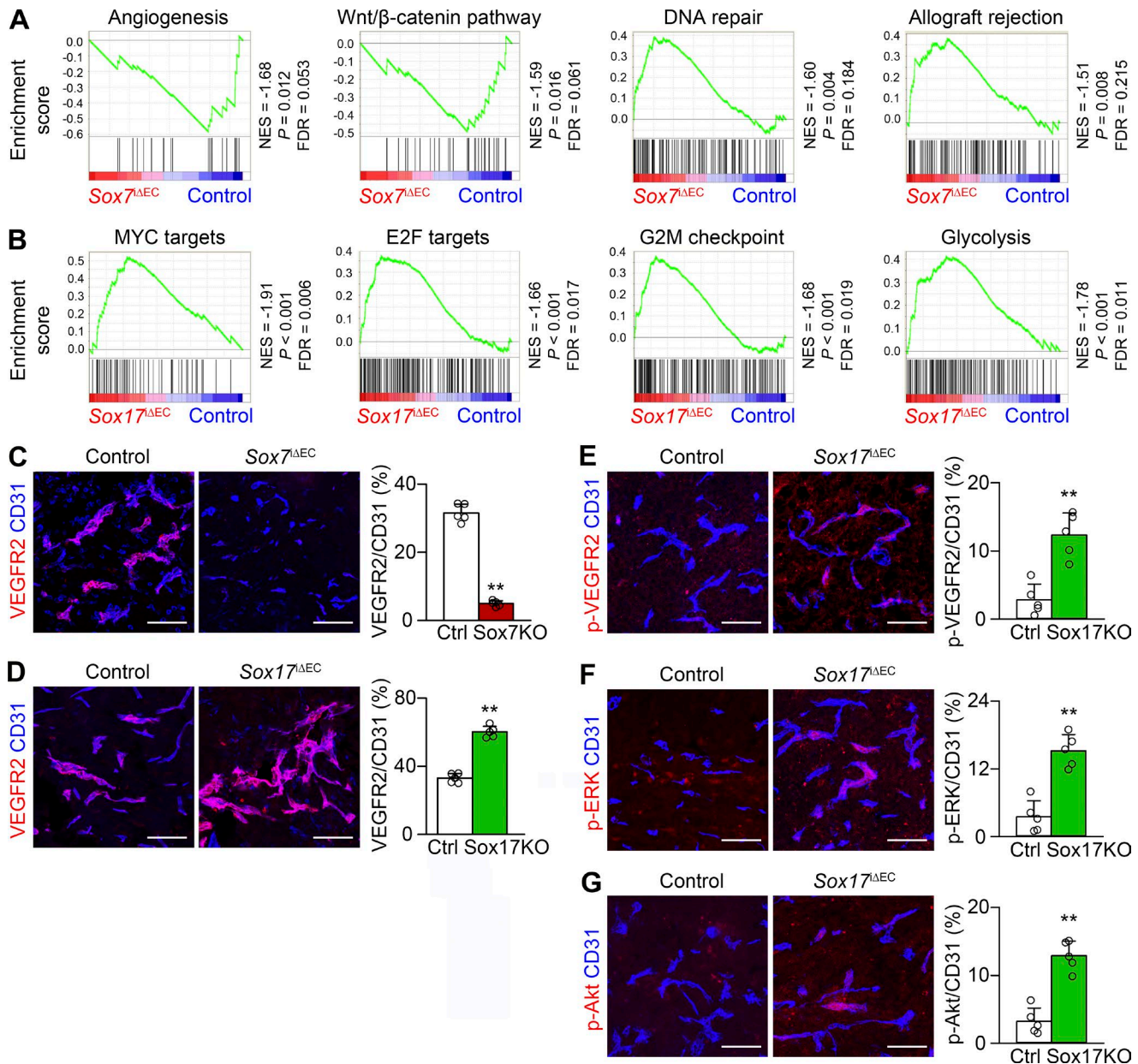
Figure 7. **Sox7 up-regulates and Sox17 down-regulates VEGFR2 in HGG vessels. (A and B)** GSEA of differentially expressed genes in *Sox7*-deficient (A) and *Sox17*-deficient (B) tECs compared with controls according to RNA sequencing. FDR, false discovery rate; NES, normalized enrichment score. **(C–G)** CD31-positive HGG vessels. (C) Repressed VEGFR2 in *Sox7*$^{\Delta EC}$ (S7KO) mice. (D–G) Enhanced VEGFR2 (D), phosphor (p)-VEGFR2 (E), p-ERK (F), and p-Akt (G) in *Sox17*$^{\Delta EC}$ (S17KO) mice. Values are presented as mean ± SD (*n* = 5). **, P < 0.01. Bars, 100 µm.

Sox7 expression in tumor vessels is associated with poor prognosis and impaired vasculature in grade IV glioma patients
We studied the clinical relevance of Sox7 in HGG. Grade IV glioma patients were divided into two groups based on Sox7 expression in tumor vessels, implying endothelial heterogeneity in HGG. Among 189 patients, Sox7 was detectable in the tumor vessels of 62 Sox7-positive patients (Fig. 10 A). Of the 127 Sox7-negative patients, 71% expressed a high level of Sox17 in tumor vessels, but only 23% of Sox7-positive patients expressed Sox17 at a high level (Fig. 10 A), indicating an inverse relationship between Sox7 and Sox17 expression. Compared with Sox17-high tumor vessels, Sox7-positive tumor vessels were small and well branched (Fig. 10 B). Overall survival and progression-free survival were

significantly poorer in the Sox7-positive population compared with the Sox7-negative population (Fig. 10, C and D; and Fig. S4 A). In contrast, when patients were divided based on Sox17 expression in tumor vessels, the Sox17-high and Sox17-low patient populations exhibited no difference in overall and progression-free survival (Fig. S4, B and C).

Patient groups with Sox7-positive tumor vessels exhibited poorer symptoms and a higher degree of peritumoral edema in the circumferential region at diagnosis compared with the other group (Fig. S4, D and E), suggesting more vessel leakage in the Sox7-positive population. Consistently, the Sox7-positive patients tended to have abundant hemorrhage in specimens relative to Sox7-negative patients (Fig. 10, E and I). Dynamic
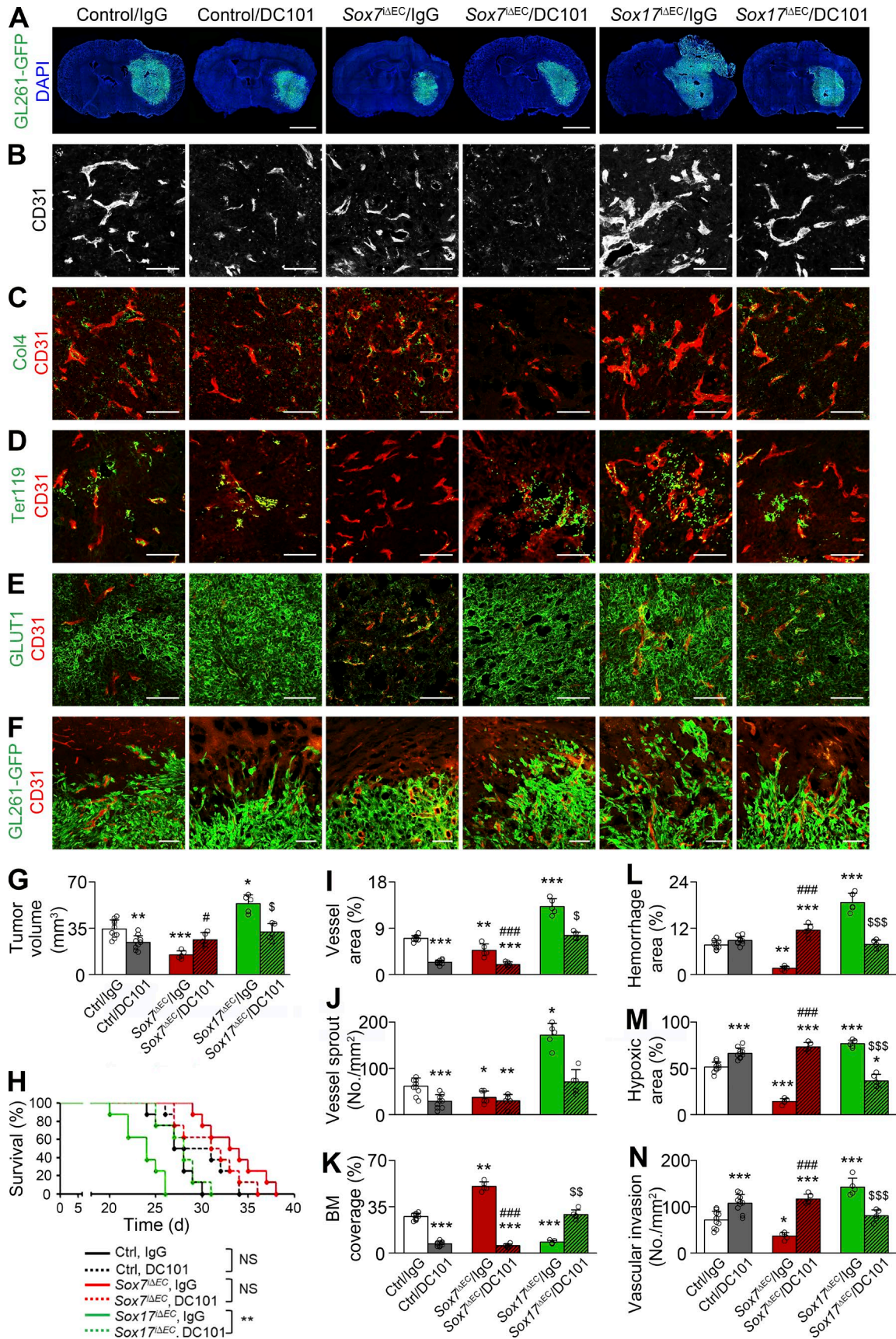
contrast-enhance (DCE) magnetic resonance (MR) imaging and accompanying flow decay mapping also showed more intratumoral leakage and peritumoral edema in Sox7-positve patients relative to Sox7-negative patients (Fig. 10, F, H, J, and L; and Fig. S4 F). On perfusion MR imaging, Sox7-positive patients had prominent blood flow within the tumor relative to Sox7-negative patients (Fig. 10, G and K; and Fig. S4 G), implying more severe tumor malignancy and abnormally enhanced vessel area in Sox7-positive patients. These findings indicate that the Sox7-positive patients have more severely impaired intratumoral vascular function than the others. Collectively, these clinical data based on a large HGG patient population reveal the heterogeneity of Sox7 expression, present Sox7 as a vascular marker of poor prognosis, and implicate Sox7 in tumor vessel abnormality.

Discussion

In this study, we revealed that two homologous transcription factors, Sox7 and Sox17, broadly contrast across expression, function, and therapeutic response in orthotopic HGG models (Fig. S4 H). Activated Sox7 promotes vascular abnormalities, such as tumor angiogenesis, vessel destabilization, vasodilation, and impaired vascular function, subsequently leading to tumor hypoxia and tumor growth. In contrast, Sox17 in HGG vessels antagonizes these malignant changes. VEGFR2 inhibition delays tumor growth by normalizing Sox17-deficient vessels with high levels of Sox7 but promotes tumor growth by impairing Sox7-deficient vessels. In the human HGG patient population, Sox7 is expressed in one-third of patients with poor clinical outcome and impaired tumor vascular function.

HGG is characterized by angiogenic vessels, and several processes, such as sprouting, vascular differentiation from cancer stem cells, and vascular mimicry, have been suggested as potential angiogenic mechanisms (Jain et al., 2007; Wang et al., 2010; Cheng et al., 2013; Das and Marsden, 2013). However, the precise mechanisms of its tumor angiogenesis remain elusive because vessel cooption, rather than angiogenesis, is the main vessel characteristic of animal HGG models (Blouw et al., 2003; Bergers and Hanahan, 2008; Du et al., 2008). The general mechanism of tumor angiogenesis has been established based on angiogenic tumor models, such as spontaneous pancreatic islet tumors, orthotopic breast tumors, and subcutaneous ectopic tumors (Carmeliet and Jain, 2011; Hanahan and Weinberg, 2011; Saharinen et al., 2011). The limited benefit of antiangiogenic therapy in HGG patients may be ascribed to the lack of knowledge on HGG angiogenesis.

We found that sprouting angiogenesis is inactive in intracranial HGG grown in wild-type mice. However, endothelial Sox17 deletion activated tumor angiogenesis as shown by abundant vascular sprouts and tip cells, indicating that Sox17 masks an angiogenic activity in HGG. In contrast, Sox17 promotes tumor angiogenesis in subcutaneous ectopic tumors (Yang et al., 2013). Regardless of the type of tumor cells, GL261- and LLC-derived tumors grown in a subcutaneous region exhibit strong Sox17 expression, but the same tumors grown in the brain express Sox17 only modestly. Similarly, transcription factor HIF-1α–deficient HGG cells elicit different vessel changes depending on the implantation site, being better vascularized when transplanted intracranially and poorly vascularized in subcutaneous environment (Blouw et al., 2003). These findings suggest that there is a mechanism of tumor angiogenesis specific to tumors grown in the brain. In contrast to their opposing expression and function in intracranial tumors, Sox7 and Sox17 exhibit overlap in expression and function and jointly promote developmental angiogenesis in the postnatal brain (Kim et al., 2016). These findings suggest that Sox7 and Sox17 can choose different relationships even in the same brain region depending on the vascular context. Likewise, homologous transcription factors Irx3 and Irx5 have a cooperative role in embryonic cardiac morphogenesis but an antagonistic role in postnatal cardiac conduction (Gaborit et al., 2012). Together, the tumor as a pathological factor and the brain as a regional factor set the opposing expression and function of Sox7 and Sox17 for HGG angiogenesis.

Contrasting Sox7 and Sox17 expression in HGG vessels is sculpted by Dll4 signaling and their epistatic regulation; Dll4 repressed Sox17 expression and Sox17 repressed Sox7 expression in tECs. Thus, Dll4 up-regulation promotes the expression of proangiogenic factor Sox7 via Sox17 repression. Consistently, Dll4 deletion decreased vascular area in intracranial HGG. On the contrary, Dll4 blocking is known to promote nonproductive tumor angiogenesis in subcutaneous tumor models via unknown mechanisms (Noguera-Troise et al., 2006; Ridgway et al., 2006), suggesting that Dll4 signaling regulates tumor angiogenesis differently depending on the tumor type. The regulatory cascade in tECs continues to VEGFR2; Sox7 promoted VEGFR2 expression, but Sox17 repressed it. In general, VEGFR2 is fundamental for vessel abnormalities in various tumors (Carmeliet and Jain, 2011; Saharinen et al., 2011). VEGFR2 levels in tumor vessels also correlated with vessel abnormality, hypoxia, and tumor growth in HGG models. Importantly, tumor angiogenesis, vessel destabilization, and tumor growth promoted by Sox17 deletion were rescued by either Sox7 deletion or VEGFR2 inhibition, verifying their functional relationship. Our study established that the

Figure 8. **Vascular and tumor responses to VEGFR2 inhibition are variable according to Sox7 levels in HGG vessels.** Control (Ctrl), Sox7^{ΔEC} (S7KO), and Sox17^{ΔEC} (S17KO) mice bearing HGG were administered with control (IgG) or α-VEGFR2 (DC101) Ab. **(A)** GL261-GFP HGGs. **(B–F)** CD31-positive HGG vessels. (B) Vascular network. (C) Col4-positive basement membrane (BM). (D) Ter119-positive erythrocytes. (E) GLUT1 immunostaining. (F) Invasion of GL261-GFP tumor cells at the tumor periphery. **(G)** Quantification of tumor volume in A. **(H)** Survival curves for HGG-bearing mice (n = 8). **(I and J)** Quantification of vessel area (I) and sprouts (J) in B. **(K)** Quantification of coverage in C. **(L)** Quantification of hemorrhage in D. **(M)** Quantification of hypoxic area in E. **(N)** Quantification of perivascular invasion in F. Values are presented as mean ± SD (n = 5 unless otherwise denoted). *, P < 0.05; **, P < 0.01; ***, P < 0.001 versus control/IgG; #, P < 0.05; ###, P < 0.001 versus Sox7^{ΔEC}/IgG; $, P < 0.05; $$, P < 0.01; $$$, P < 0.001 versus Sox17^{ΔEC}/IgG (log-rank test). NS, not significant. Bars: 2 mm (A); 100 µm (B–F).

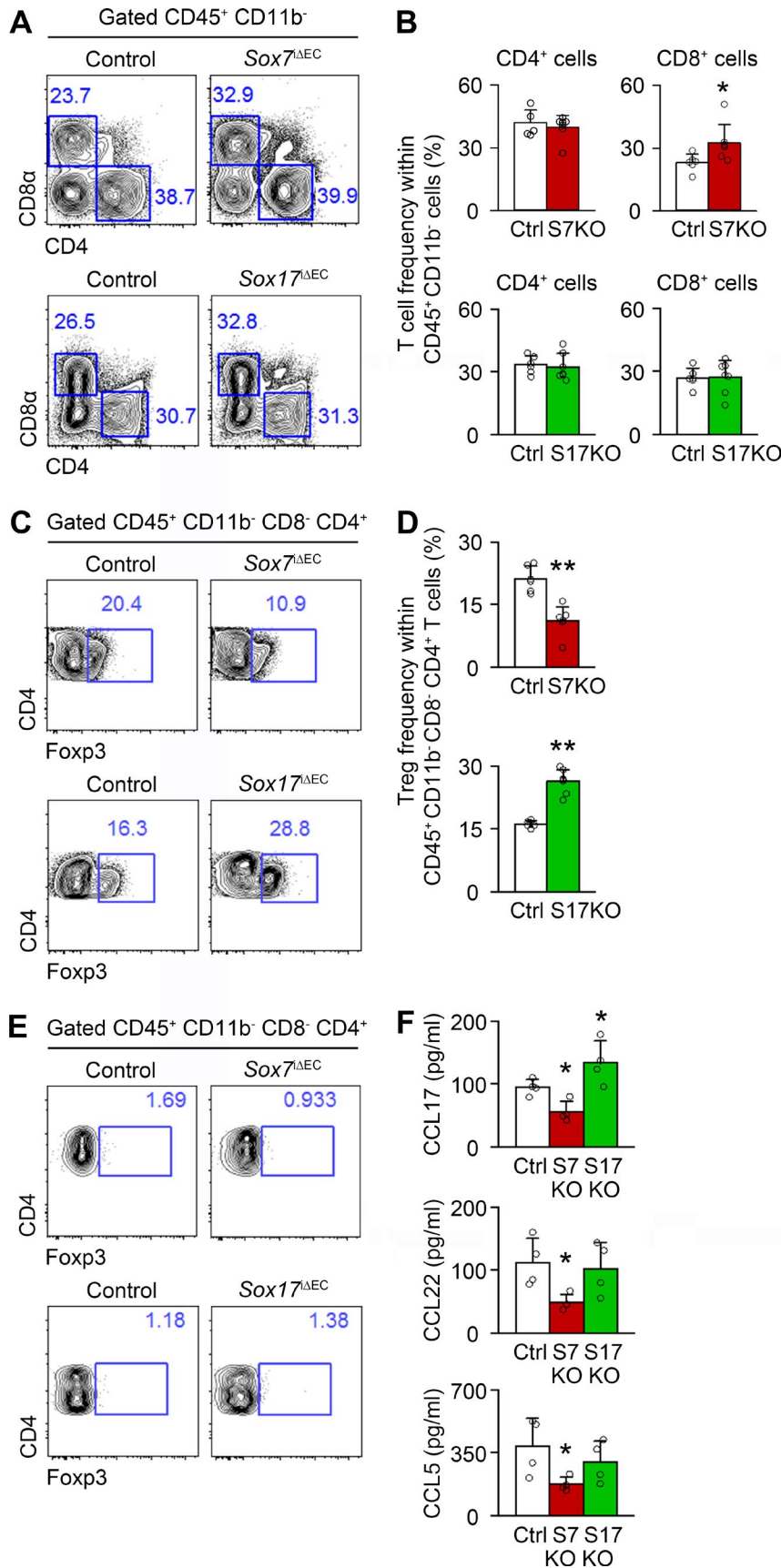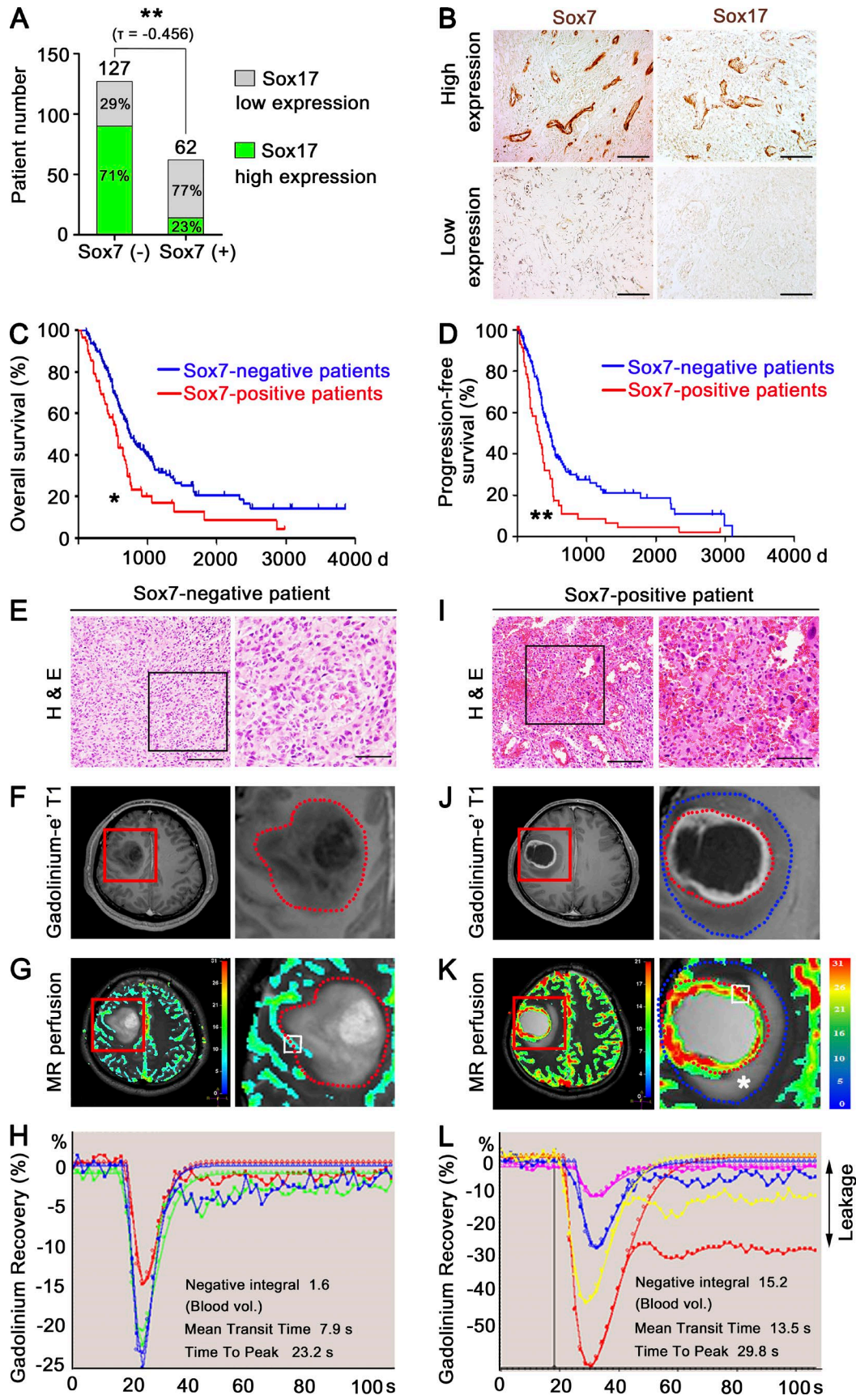Sox7–VEGFR2 axis drives tumor angiogenesis, vessel abnormalization, and tumor growth in HGG, and Sox17 antagonizes these processes by repressing Sox7 expression.

Immune suppression is a key process for tumor growth, and T reg cells inhibit T cell–mediated immunity in a range of tumors (Nishikawa and Sakaguchi, 2014). T reg cells were also abundant in our HGG models. Importantly, *Sox7* deletion decreased the T reg cell frequency and delayed tumor growth, whereas *Sox17* deletion increased T reg cell abundance and promoted tumor growth, suggesting that Sox7 and Sox17 control tumor progression in part via T reg cells. Several studies have reported that hypoxia and glucose shortage can exacerbate immune suppression in tumors (Clambey et al., 2012; Barsoum et al., 2014). Enhanced oxygen and glucose supply by *Sox7*-deficient vessels may foster a tumor environment favorable for T cell–mediated immunity.

Sox7 and Sox17 induce opposing responses to VEGFR2 inhibition. Regarding the absence or presence of therapeutic outcome of antiangiogenic therapy, HGG patients can be categorized into two groups: the nonresponder, which is intrinsically refractory to therapy, and the responder (Batchelor et al., 2007; Chinot et al., 2014; Gilbert et al., 2014). However, in several studies based on animal models, anti-VEGF therapies induce a single pattern of response in HGG rather than dichotomy; it transiently delays tumor growth but soon induces adaptive resistance, such as enhanced tumor invasiveness, leading to tumor recurrence (Batchelor et al., 2007; Bergers and Hanahan, 2008; Lu et al., 2012; Scholz et al., 2016). Thus, how antiangiogenic therapy can elicit different therapeutic outcomes remains unknown. In this study, α-VEGFR2 Ab produces three different patterns of response in survival and resistant glioma invasion: increased survival with proinvasive adaptation in the control, decreased survival with aggressively enhanced invasion in the group lacking endothelial *Sox7*, and increased survival with less invasion in the group lacking endothelial *Sox17*. Whereas α-VEGFR2 Ab induces rarefaction of *Sox7*-deficient HGG vessels with less abnormality, it stabilizes *Sox17*-deficient HGG vessels with aberrant angiogenesis and severe abnormality. These vessel changes subsequently affect tumor hypoxia and, finally, tumor invasiveness. Interestingly, this hypoxic-driven tumor invasion is often observed in the vessel cooption mediating resistance to anti-VEGF therapy in several tumor contexts such as HGG and liver metastases (Lu et al., 2012; Frentzas et al., 2016). In our HGG models, VEGFR2 blocking decreased endothelial Dll4 expression (Fig. S5 D), which can subsequently induce several vessel changes, including Sox7 and Sox17 expression. Further studies will reveal detailed molecular mechanisms for the heterogeneous response to α-VEGFR2 Ab. Our findings suggest that variable vascular and tumor responses to α-VEGFR2 Ab are attributed to heterogeneous vessel abnormality, which is regulated by Sox7 and Sox17.

Our findings suggest that a small subset hidden in the nonresponder group may have an immediate adverse outcome, rather than indifference, to α-VEGFR2 Ab, suggesting that the range of heterogeneity in therapeutic response to antiangiogenic therapy may be wider than currently thought. However, anti-VEGF therapy could give a better clinical outcome such as significantly enhanced overall survival to a subpopulation, which in particular has a severe vascular abnormality. In this regard, predictive biomarkers, which are now missing, may improve the efficacy of anti-VEGF therapy by selecting suitable patient group. In contrast to transient vessel normalization by antiangiogenic therapy (Jain et al., 2007; Saharinen et al., 2011; Van der Veldt et al., 2012), α-VEGFR2 Ab induces enduring normalization in *Sox17*-deficient HGG vessels, suggesting its combination with chemotherapy for additional therapeutic benefit. Our study also suggests that ramucirumab, an α-VEGFR2 Ab approved for the treatment of gastric cancer and non–small cell lung cancer (Fuchs et al., 2014; Garon et al., 2014; Wilke et al., 2014), is suitable for indication expansion to HGG because it effectively delays tumor growth by normalizing tumor vessels in a certain tumor context.

Importantly, we verified clinical relevance of Sox7 in HGG patients. Although HGG is divided into subtypes based on histopathologic and molecular analysis (Verhaak et al., 2010; Brennan et al., 2013), its vascular pattern remains entangled as a result of its high degree of heterogeneity. We divided HGG patients on the immunohistologic basis of Sox7 expression in tumor vessels. High Sox7 levels correlated with hyper-leakage and predicted poor prognosis of patients. These results suggest that Sox7 promotes vessel abnormality and, consequently, tumor growth in HGG patients. Similar to mouse HGG models, the expression of Sox7 and Sox17 exhibited an inverse relationship in specimens from HGG patients. However, Sox17 levels are independent from prognosis of patients. A future study will elucidate the role of Sox17 in total HGG consisting of various subtypes. Given only a few prognostic markers available for HGG, such as methylation of methylguanine methyltransferase promoter (Hegi et al., 2005) and IDH1 mutation (Yan et al., 2009) on the basis of tumor heterogeneity, our findings provide an insight into an alternative option for prognostic markers based on endothelial heterogeneity. Though endothelial Sox7 was detected in one-third of HGG patients, we found nonendothelial Sox7 expression in some human HGG sections. As a result of a wide range of intra- and intertumoral heterogeneities, we were not able to characterize the pattern of nonendothelial Sox7 expression in human HGG.

Figure 10. **Sox7 expression in tumor vessels correlates with poor prognosis and impaired tumor vessels of grade IV glioma patients. (A)** Categorization of grade IV glioma patients based on Sox7 levels in tumor vessels. **(B)** Immunostaining for Sox7 and Sox17. **(C and D)** Overall survival (C) and progression-free survival (D) of Sox7-positive (n = 62) and Sox7-negative (n = 127) patients. *, P < 0.05; **, P < 0.01 (log-rank test). **(E–L)** Representative images of Sox7-negative (E–H) and Sox7-positive (I–L) patients. (E and I) H&E images (left). Enlarged images of boxed area (right). (F and J) DCE MR images (left) and enlarged views of red-lined box (right). (G and K) Perfusion MR images (left) and enlarged views of red lined box (right). Insets are regions for measuring flow decay. Color index denotes the intensity of blood flow signal. Red dotted lines: tumor margin. Blue dotted lines: peritumoral edema margin. Asterisk denotes copious peritumoral leakage. (H and L) Negative integral map showing blood flow decay at multiple regions. Each line denotes the dynamic flow signal from single inset in G and K (right). Delayed signal recovery indicates vessel leakage caused by poor removal of extravasated gadolinium. See Fig. S4 (F and G) for quantitation of intratumoral leakage (F, H, J, and L) and tumor perfusion (G and K), respectively. Bars: 100 µm (B, E [right], and I [right]); 200 µm (E, left; I, left).

Further investigation based on advanced models will elucidate additional roles of Sox7 in HGG.

In summary, Sox7 promotes tumor angiogenesis in HGG by up-regulating VEGFR2. HGG exhibits a variable therapeutic response to α-VEGFR2 Ab depending on Sox7 level in tumor vessels. For clinical relevance, high Sox7 levels predict poor survival, early recurrence, and impaired tumor vascular function in HGG patients. Our study identifies a novel proangiogenic factor Sox7 for HGG and proposes that Sox7 might have potential as a predictive biomarker for antiangiogenic therapy.

Materials and methods

Study design
The overall objective of this controlled laboratory experimental study was to investigate the role of Sox7 and Sox17 in mouse HGG models. We used targeted mouse models with intracranially implanted glioma cells. We treated tumor-bearing mice with α-VEGFR2 Ab to evaluate therapeutic outcome to antiangiogenic treatment. Vascular morphology, leakage, perfusion, and hypoxia were assessed by confocal microscopy. Sample size was determined by the statistical software PASS 12 (power analysis and sample size) using the preliminary dataset to detect a difference in means between experimental and control groups. No special but general randomized determination was used for animal allocation. All data were included, and investigators were not blinded for the animal study. All animal experiments were approved by the Animal Care Committee of Korea Advanced Institute of Science and Technology (KA2013-41). In addition, a retrospective cohort of HGG patients was evaluated for Sox7 and Sox17 expression under approval by the Institutional Review Board of Asan Medical Center (2011-1012). The grade IV glioma patients with the standard therapy were enrolled in this study by excluding patients with palliative treatments. Correlation of Sox7 and Sox17 levels with prognosis and vascular function of patients was evaluated.

Tumor models and treatment regimens
The murine GL261 glioma line was obtained from K. Plate (Goethe University Medical School, Frankfurt, Germany). The GL261-GFP glioma cell line was generated by transducing GL261 cells with lentivirus carrying GFP-expressing vector. LLC cells were obtained from the American Type Culture Collection. 83NS patient-derived glioblastoma stem cells were maintained as described previously (Yin et al., 2017). No mycoplasma was detected in the cell cultures. For intracranial tumor models, 2 × 10^5 GL261, 2 × 10^5 GL261-GFP, 2 × 10^5 LLC cells, and 5 × 10^5 83NS cells were implanted into the right hemispheres of 8–10-wk-old male experimental mice via stereotaxic injection. For subcutaneous tumor models, suspensions of GL261 or LLC (10^6 cells in 100 µl) were subcutaneously injected into the dorsal flank of 8–10-wk-old male experimental mice. Littermates were used in all experiments. We generated the constructs for α-Dll4 Ab based on the sequence of the variable regions of clone 26.82 (US 7803377 B2) and validated its efficacy via excessive postnatal retina angiogenesis (Fig. S5 A). We also validated the efficacy of α-VEGFR2 Ab (DC101) by inhibited postnatal retina angiogenesis

(Fig. S5 B). To block Dll4 and VEGFR2, 5 mg/kg α-Dll4 Ab, 40 mg/kg DC101, or an equal amount of their control Abs was injected into tumor-bearing mice (Fig. S5 C). To measure tumor volume, at least eight coronal brain sections were prepared every 100 µm, placing bregma in the center section. Among the eight brain slices, the section with the largest tumor was selected, and tumor volume was calculated according to the formula $0.5 × A × B^2$, where A is the longest diameter of a tumor, and B is its perpendicular diameter.

Statistical analysis
Experimental values are presented as mean ± SD unless otherwise indicated. Significance was determined by the Mann-Whitney U test between two groups or the Kruskal-Wallis test followed by the Tukey's HSD (honest significant difference) test with ranks for more than three groups. Survival curves were evaluated using the Kaplan-Meier method, and statistical differences were determined using the log-rank test. Statistical analyses were performed using PASW statistics 18 (SPSS). P < 0.05 was considered significant.

Mice
The $Cdh5$(BAC)-CreER[T2] model was obtained from Y. Kubota (Keio University, Tokyo, Japan). $Sox7^{mCh/+}$ (Kim et al., 2016), $Sox7^{fl/+}$ (Kim et al., 2016), $Sox17^{GFP/+}$ (Kim et al., 2007), $Sox17^{fl/+}$ (Kim et al., 2007), $Dll4^{fl/+}$ (Hozumi et al., 2008), and $Cdh5$(BAC)-CreER[T2] (Okabe et al., 2014) mice were housed in a pathogen-free animal facility. All mouse lines were backcrossed onto the C57BL/6 background at least 10 times. To excise $Sox7$, $Sox17$, and $Dll4$ in ECs, the $Cdh5$(BAC)-CreER[T2] driver line was bred with $Sox7^{fl/fl}$, $Sox17^{fl/fl}$, and $Dll4^{fl/fl}$ mice, and experimental mice were intraperitoneally administered 20 mg/kg tamoxifen (Sigma). Mice were anesthetized with 80 mg/kg ketamine and 12 mg/kg xylazine, and their brains were harvested for further analyses. All animal experiments were approved by the Animal Care Committee of Korea Advanced Institute of Science and Technology (KA2013-41).

Histological analyses
For H&E staining, tumors and indicated organs were fixed overnight in 4% paraformaldehyde (PFA), embedded in paraffin, and cut into 3-µm sections. For immunofluorescence, samples were fixed in 1% PFA, dehydrated in 20% sucrose solution overnight, and embedded in tissue-freezing medium (Leica). Frozen blocks were cut into 30-µm sections. Tissue sections were blocked in PBST (0.3% Triton X-100 in PBS) with 5% goat or donkey serum and incubated with the following primary Abs: α–mouse CD31 (hamster [2H8; Millipore] or rat [MEC13.3; BD Biosciences]), α–human CD31 (rabbit polyclonal; Abcam), α-Sox7 (goat; R&D Systems), α-Sox17 (goat; R&D Systems), α-PDGFRβ (rat; clone APB5; eBioscience), α–collagen type IV (rabbit; Cosmo Bio), α-Ter119 (rat; eBioscience), α-GLUT1 (rabbit; Millipore), α-VEGFR2 (goat; R&D Systems), α-ZO-1 (rabbit; Invitrogen), α–VE-cadherin (rat; BioLegend), α-PH3 (rabbit; Millipore), α-Caspase3 (rabbit; Millipore), α–phospho-VEGFR2 (rabbit; Cell Signaling), α–phospho-ERK (rabbit; Cell Signaling), or α–phospho-Akt (rabbit; Cell Signaling). After several washes, sections were incubated with the following secondary Abs: Alexa Fluor 488–, Alexa Fluor 596–,

or Alexa Fluor 647–conjugated α–hamster IgG, Alexa Fluor 488– or Alexa Fluor 596–conjugated α–rabbit IgG, Alexa Fluor 488– or Alexa Fluor 596–conjugated α–rat IgG (Jackson ImmunoResearch), or Alexa Fluor 488– or Alexa Fluor 596–conjugated α–goat IgG (all Jackson ImmunoResearch). Nuclei were stained with DAPI (Invitrogen). The samples were then mounted with fluorescent mounting medium (DAKO), and immunofluorescent images were obtained using confocal microscope (LSM780; Zeiss).

Assessment of vascular leakage, perfusion, and hypoxia

To analyze vascular leakage, 8 ml/kg Evans blue solution (0.5%; Sigma) was injected intravenously 24 h before brains were harvested. To analyze vascular perfusion, 0.1 mg DyLight 488–conjugated tomato lectin (Vector Laboratory) was injected intravenously 30 min before brains were harvested. To detect the tumor hypoxic area, 60 mg/kg pimonidazole hydrochloride (Natural Pharmacia International) was injected intraperitoneally 60 min before brains were harvested. Mice were anesthetized and perfused by intracardiac injection of 1% PFA to remove circulating Evans blue, lectin, and pimonidazole. Tumors were then harvested, sectioned, and stained with FITC-conjugated antihypoxyprobe Ab.

Morphometric and densitometric analyses

Vessel area was calculated as the CD31-positive area per random 0.54-mm² regions. The number of vessels and vascular branches were counted in random 0.54-mm² regions. Vessel diameter and the number of vascular sprouts (>10 μm in length) were measured in random 0.13-mm² regions. Vascular tortuosity was calculated as described previously (Scott et al., 2014). Expression levels of Sox7, Sox17, Sox7-mCherry, Sox17-GFP, Dll4, and VEGFR2 were determined as percentages of the corresponding fluorescent-positive area per CD31-positive blood vessel. Coverage of PDGFRβ-positive pericyte, collagen type IV–positive basement membrane, and VE-cadherin–positive adherens junctions were calculated as the percentages of corresponding fluorescent-positive length along the CD31-positive blood vessels in random 0.54-mm² regions. Vascular perfusion was quantified as the percentage of FITC-lectin–positive area divided by CD31-positive area per random 0.54-mm² regions. Hemorrhage, vascular leakage, hypoxic area, and apoptotic area were quantified as the percentages of Ter119-, Evans blue–, GLUT1-, and caspase 3–positive area, respectively, per random 0.54-mm² regions. The densities of immunofluorescence signals were quantified using ImageJ software (National Institutes of Health).

Flow cytometry

We performed flow cytometric analysis as described previously (Oh et al., 2017a). In brief, single cells were pretreated with α-CD16/32 Ab (2.4 G; TONBO Bioscience) and stained with the following Abs: α–mouse Foxp3 (FJK-16s; eBioscience), α–mouse CD8α (53-6.7; BD Biosciences), α–mouse CD11b (M1/70; BD Biosciences), α–mouse CD4 (GK1.5; BioLegend), or α–mouse CD45.2 (104; TONBO Bioscience). For T reg cell staining, Foxp3 was stained using the Foxp3/Transcription factor staining buffer set (eBioscience) according to the manufacturer's protocol. The stained cells were analyzed by cell analyzers (LSR

Fortessa or LSR II; BD Biosciences). All data were analyzed using FlowJo (TreeStar).

ELISA

We assessed the protein levels of CCL5, CCL17, and CCL22 using previously described methods with slight modification (Oh et al., 2017b). In brief, brain hemispheres containing GL261 HGG were chopped into small pieces in PBS with protease inhibitor (Roche). Tissue samples were homogenized by an ultrasonic dismembrator. After the samples were centrifuged at 3,000 g for 15 min at 4°C, the supernatants were collected and stored at –80°C. CCL5, CCL17, and CCL22 were measured using ELISA kits (R&D Systems) according to the manufacturer's protocol.

Sorting of tECs

GL261-derived HGGs were broken into small pieces, incubated in buffer containing 0.1% collagenase type 1A (Worthington) and 3 U/ml DNase I (Worthington) for 50 min at 37°C, strained with a 40-μm nylon mesh to remove cell clumps, and incubated in lysis buffer for 2 min to remove erythrocytes. Single-cell suspensions were incubated for 30 min with biotin-conjugated α-CD31 Ab (rat; 390; Miltenyi), washed, and incubated for 20 min with α-biotin microbeads (Miltenyi). CD31-positive cells were enriched using an autoMACS Pro separator (Miltenyi). Enriched cells were further stained with the following Abs: PE-conjugated α–mouse CD31 (rat; MEC 13.3; BioLegend), APC-conjugated α–mouse CD45 (rat; 30-F11; BioLegend), and APC-conjugated α–mouse Ter119 (rat; BioLegend). To discriminate dead cells, cells were stained with DAPI (Sigma) and purified by a flow cytometer (FACSAria II; BD Biosciences).

RNA sequencing and data analysis

For control and test RNA, the library was constructed using SEN SE mRNA-Seq Library Prep kit (Lexogen) according to the manufacturer's instructions. In brief, mRNA was isolated from 2 μg of total RNA by oligo-dT magnetic beads and hybridized with starter/stopper heterodimers containing Illumina-compatible linker sequences. Reverse transcription, ligation of newly synthesized cDNA inserts to the stopper, and second strand synthesis were performed serially to generate the library. High-throughput sequencing was performed as paired-end 100 sequencing using a HiSeq 2000 sequencing system (Illumina).

RNA sequencing reads were mapped using the TopHat software tool to obtain the alignment file, which was used to assemble transcripts, estimate their abundance, and detect differential expression of genes or isoforms using cufflinks. Clustering and heat map construction were performed using Cluster and Treeview as described previously (Eisen et al., 1998). Gene ontology and the ingenuity pathway analysis (QIAGEN) was performed for the prediction of biological and signaling changes. GSEA software was used to identify the differences in expressed gene sets between study and control groups (Subramanian et al., 2005). We compared gene expression levels between Sox7-deficient tECs (n = 2) and controls (n = 2) and between Sox17-deficient tECs (n = 3) and controls (n = 3). Poorly expressed genes in both the study and control groups were filtered out using two criteria: maximum read count <100 and median read count <10. Next, twofold up-regulated or down-regulated genes were selected as

differentially expressed genes. Thus, 2,165 (1,218 up-regulated and 947 down-regulated) and 1,756 (861 up-regulated and 895 down-regulated) genes were differentially expressed in *Sox7*- and *Sox17*-deficient tECs, respectively. Raw data were uploaded to the Gene Expression Omnibus database of the National Center for Biotechnology Information (GSE90459 and GSE107530).

Patient enrollment and specimen collection

Among 440 patients diagnosed as grade IV glioma upon radiological examination, 277 patients were confirmed pathologically as having primary glioblastoma. By excluding 88 patients with palliative treatments, 189 patients treated with the standard therapy (surgical removal and concurrent chemoradiation therapy) were collected and reviewed in this study. All human studies were approved by the Institutional Review Board of Asan Medical Center (2011-1012), and all patient samples were collected with written informed consent.

DCE MR imaging

Imaging was performed on a 3.0-T MP25 Ingenia (Philips). For DCE perfusion MR imaging, three-dimensional gradient-echo data with 21 sections were obtained before, during, and after the administration of 0.1 mmol/kg gadoterate meglumine at a rate of 4 ml/s. The dynamic acquisition was performed with a temporal resolution of 3.22 s, and contrast agent was administered after 10 baseline dynamic acquisitions (total of 120 dynamic acquisitions). The detailed imaging parameters for DCE perfusion MR imaging were as follows: 6.4/3.1; flip angle, 15°; field of view, 24 cm; section thickness, 4 mm; gap, none; and matrix, 184 × 186. The total acquisition time for DCE MR imaging was 5 min and 41 s. These procedural images were aimed to cover the entire tumor. Data processing was performed using a postprocessing workstation (Philips Medical Systems). Normalized signal intensity was plotted against time for the corresponding normal brain on the contralateral side and the lesion. The plot lines represent the fitted curves derived using the first-pass PM (photon mapping) algorithm. The percent signal recovery was obtained to measure tumor vessel leakage (Chen et al., 2016).

Online supplemental material

Fig. S1 shows that Sox7 and Sox17 levels with an inverse relationship categorize HGG vessels by morphology. Fig. S2 shows that *Sox7* and *Sox17* deletion induce opposite changes on HGG and its vessels. Fig. S3 shows that *Sox7* and *Sox17* deletion have no effect on nontumor brain vessels. Fig. S4 shows that Sox7 expression correlates with poor symptoms and a higher degree of tumor leakage of grade IV glioma patients. Fig. S5 depicts the validation of α-Dll4 and α-VEGFR2 Abs.

References

Barsoum, I.B., C.A. Smallwood, D.R. Siemens, and C.H. Graham. 2014. A mechanism of hypoxia-mediated escape from adaptive immunity in cancer cells. *Cancer Res.* 74:665–674. https://doi.org/10.1158/0008-5472.CAN-13-0992

Batchelor, T.T., A.G. Sorensen, E. di Tomaso, W.-T. Zhang, D.G. Duda, K.S. Cohen, K.R. Kozak, D.P. Cahill, P.-J. Chen, M. Zhu, et al. 2007. AZD2171, a pan-VEGF receptor tyrosine kinase inhibitor, normalizes tumor vasculature and alleviates edema in glioblastoma patients. *Cancer Cell.* 11:83–95. https://doi.org/10.1016/j.ccr.2006.11.021

Bergers, G., and D. Hanahan. 2008. Modes of resistance to anti-angiogenic therapy. *Nat. Rev. Cancer.* 8:592–603. https://doi.org/10.1038/nrc2442

Blouw, B., H. Song, T. Tihan, J. Bosze, N. Ferrara, H.-P. Gerber, R.S. Johnson, and G. Bergers. 2003. The hypoxic response of tumors is dependent on their microenvironment. *Cancer Cell.* 4:133–146. https://doi.org/10.1016/S1535-6108(03)00194-6

Brennan, C.W., R.G. Verhaak, A. McKenna, B. Campos, H. Noushmehr, S.R. Salama, S. Zheng, D. Chakravarty, J.Z. Sanborn, S.H. Berman, et al. TCGA Research Network. 2013. The somatic genomic landscape of glioblastoma. *Cell.* 155:462–477. https://doi.org/10.1016/j.cell.2013.09.034

Carmeliet, P., and R.K. Jain. 2011. Molecular mechanisms and clinical applications of angiogenesis. *Nature.* 473:298–307. https://doi.org/10.1038/nature10144

Chen, H., N. Liu, Y. Li, F. Chen, and G. Zhu. 2016. Permeability imaging in cerebrovascular diseases: applications and progress in research. *Neurovasc. Imaging.* 2:1. https://doi.org/10.1186/s40809-016-0015-4

Cheng, L., Z. Huang, W. Zhou, Q. Wu, S. Donnola, J.K. Liu, X. Fang, A.E. Sloan, Y. Mao, J.D. Lathia, et al. 2013. Glioblastoma stem cells generate vascular pericytes to support vessel function and tumor growth. *Cell.* 153:139–152. https://doi.org/10.1016/j.cell.2013.02.021

Chinot, O.L., W. Wick, W. Mason, R. Henriksson, F. Saran, R. Nishikawa, A.F. Carpentier, K. Hoang-Xuan, P. Kavan, D. Cernea, et al. 2014. Bevacizumab plus radiotherapy-temozolomide for newly diagnosed glioblastoma. *N. Engl. J. Med.* 370:709–722. https://doi.org/10.1056/NEJMoa1308345

Clambey, E.T., E.N. McNamee, J.A. Westrich, L.E. Glover, E.L. Campbell, P. Jedlicka, E.F. de Zoeten, J.C. Cambier, K.R. Stenmark, S.P. Colgan, and H.K. Eltzschig. 2012. Hypoxia-inducible factor-1 alpha-dependent induction of FoxP3 drives regulatory T-cell abundance and function during inflammatory hypoxia of the mucosa. *Proc. Natl. Acad. Sci. USA.* 109:E2784–E2793. https://doi.org/10.1073/pnas.1202366109

Corada, M., F. Orsenigo, M.F. Morini, M.E. Pitulescu, G. Bhat, D. Nyqvist, F. Breviario, V. Conti, A. Briot, M.L. Iruela-Arispe, et al. 2013. Sox17 is indispensable for acquisition and maintenance of arterial identity. *Nat. Commun.* 4:2609. https://doi.org/10.1038/ncomms3609

Curiel, T.J., G. Coukos, L. Zou, X. Alvarez, P. Cheng, P. Mottram, M. Evdemon-Hogan, J.R. Conejo-Garcia, L. Zhang, M. Burow, et al. 2004. Specific

recruitment of regulatory T cells in ovarian carcinoma fosters immune privilege and predicts reduced survival. *Nat. Med.* 10:942–949. https://doi.org/10.1038/nm1093

Das, S., and P.A. Marsden. 2013. Angiogenesis in glioblastoma. *N. Engl. J. Med.* 369:1561–1563. https://doi.org/10.1056/NEJMcibr1309402

Du, R., C. Petritsch, K. Lu, P. Liu, A. Haller, R. Ganss, H. Song, S. Vandenberg, and G. Bergers. 2008. Matrix metalloproteinase-2 regulates vascular patterning and growth affecting tumor cell survival and invasion in GBM. *Neuro-oncol.* 10:254–264. https://doi.org/10.1215/15228517-2008-001

Eisen, M.B., P.T. Spellman, P.O. Brown, and D. Botstein. 1998. Cluster analysis and display of genome-wide expression patterns. *Proc. Natl. Acad. Sci. USA.* 95:14863–14868. https://doi.org/10.1073/pnas.95.25.14863

Francois, M., P. Koopman, and M. Beltrame. 2010. SoxF genes: Key players in the development of the cardio-vascular system. *Int. J. Biochem. Cell Biol.* 42:445–448. https://doi.org/10.1016/j.biocel.2009.08.017

Frentzas, S., E. Simoneau, V.L. Bridgeman, P.B. Vermeulen, S. Foo, E. Kostaras, M. Nathan, A. Wotherspoon, Z.H. Gao, Y. Shi, et al. 2016. Vessel co-option mediates resistance to anti-angiogenic therapy in liver metastases. *Nat. Med.* 22:1294–1302. https://doi.org/10.1038/nm.4197

Fuchs, C.S., J. Tomasek, C.J. Yong, F. Dumitru, R. Passalacqua, C. Goswami, H. Safran, L.V. Dos Santos, G. Aprile, D.R. Ferry, et al. REGARD Trial Investigators. 2014. Ramucirumab monotherapy for previously treated advanced gastric or gastro-oesophageal junction adenocarcinoma (REGARD): an international, randomised, multicentre, placebo-controlled, phase 3 trial. *Lancet.* 383:31–39. https://doi.org/10.1016/S0140-6736(13)61719-5

Gaborit, N., R. Sakuma, J.N. Wylie, K.-H. Kim, S.-S. Zhang, C.-C. Hui, and B.G. Bruneau. 2012. Cooperative and antagonistic roles for Irx3 and Irx5 in cardiac morphogenesis and postnatal physiology. *Development.* 139:4007–4019. https://doi.org/10.1242/dev.081703

Garon, E.B., T.-E. Ciuleanu, O. Arrieta, K. Prabhash, K.N. Syrigos, T. Goksel, K. Park, V. Gorbunova, R.D. Kowalyszyn, J. Pikiel, et al. 2014. Ramucirumab plus docetaxel versus placebo plus docetaxel for second-line treatment of stage IV non-small-cell lung cancer after disease progression on platinum-based therapy (REVEL): a multicentre, double-blind, randomised phase 3 trial. *Lancet.* 384:665–673. https://doi.org/10.1016/S0140-6736(14)60845-X

Gilbert, M.R., J.J. Dignam, T.S. Armstrong, J.S. Wefel, D.T. Blumenthal, M.A. Vogelbaum, H. Colman, A. Chakravarti, S. Pugh, M. Won, et al. 2014. A randomized trial of bevacizumab for newly diagnosed glioblastoma. *N. Engl. J. Med.* 370:699–708. https://doi.org/10.1056/NEJMoa1308573

Hanahan, D., and R.A. Weinberg. 2000. The hallmarks of cancer. *Cell.* 100:57–70. https://doi.org/10.1016/S0092-8674(00)81683-9

Hanahan, D., and R.A. Weinberg. 2011. Hallmarks of cancer: the next generation. *Cell.* 144:646–674. https://doi.org/10.1016/j.cell.2011.02.013

Hegi, M.E., A.-C. Diserens, T. Gorlia, M.-F. Hamou, N. de Tribolet, M. Weller, J.M. Kros, J.A. Hainfellner, W. Mason, L. Mariani, et al. 2005. MGMT gene silencing and benefit from temozolomide in glioblastoma. *N. Engl. J. Med.* 352:997–1003. https://doi.org/10.1056/NEJMoa043331

Hozumi, K., C. Mailhos, N. Negishi, K. Hirano, T. Yahata, K. Ando, S. Zuklys, G.A. Holländer, D.T. Shima, and S. Habu. 2008. Delta-like 4 is indispensable in thymic environment specific for T cell development. *J. Exp. Med.* 205:2507–2513. https://doi.org/10.1084/jem.20080134

Jain, R.K., E. di Tomaso, D.G. Duda, J.S. Loeffler, A.G. Sorensen, and T.T. Batchelor. 2007. Angiogenesis in brain tumours. *Nat. Rev. Neurosci.* 8:610–622. https://doi.org/10.1038/nrn2175

Kerber, M., Y. Reiss, A. Wickersheim, M. Jugold, F. Kiessling, M. Heil, V. Tchaikovski, J. Waltenberger, M. Shibuya, K.H. Plate, and M.R. Machein. 2008. Flt-1 signaling in macrophages promotes glioma growth in vivo. *Cancer Res.* 68:7342–7351. https://doi.org/10.1158/0008-5472.CAN-07-6241

Kim, I., T.L. Saunders, and S.J. Morrison. 2007. Sox17 dependence distinguishes the transcriptional regulation of fetal from adult hematopoietic stem cells. *Cell.* 130:470–483. https://doi.org/10.1016/j.cell.2007.06.011

Kim, K., I.-K. Kim, J.M. Yang, E. Lee, B.I. Koh, S. Song, J. Park, S. Lee, C. Choi, J.W. Kim, et al. 2016. SoxF transcription factors are positive feedback regulators of VEGF signaling. *Circ. Res.* 119:839–852. https://doi.org/10.1161/CIRCRESAHA.116.308483

Lee, S.-H., S. Lee, H. Yang, S. Song, K. Kim, T.L. Saunders, J.K. Yoon, G.Y. Koh, and I. Kim. 2014. Notch pathway targets proangiogenic regulator Sox17 to restrict angiogenesis. *Circ. Res.* 115:215–226. https://doi.org/10.1161/CIRCRESAHA.115.303142

Lu, K.V., J.P. Chang, C.A. Parachoniak, M.M. Pandika, M.K. Aghi, D. Meyronet, N. Isachenko, S.D. Fouse, J.J. Phillips, D.A. Cheresh, et al. 2012. VEGF inhibits tumor cell invasion and mesenchymal transition through a MET/VEGFR2 complex. *Cancer Cell.* 22:21–35. https://doi.org/10.1016/j.ccr.2012.05.037

Mizukami, Y., K. Kono, Y. Kawaguchi, H. Akaike, K. Kamimura, H. Sugai, and H. Fujii. 2008. CCL17 and CCL22 chemokines within tumor microenvironment are related to accumulation of Foxp3+ regulatory T cells in gastric cancer. *Int. J. Cancer.* 122:2286–2293. https://doi.org/10.1002/ijc.23392

Nishikawa, H., and S. Sakaguchi. 2014. Regulatory T cells in cancer immunotherapy. *Curr. Opin. Immunol.* 27:1–7. https://doi.org/10.1016/j.coi.2013.12.005

Noguera-Troise, I., C. Daly, N.J. Papadopoulos, S. Coetzee, P. Boland, N.W. Gale, H.C. Lin, G.D. Yancopoulos, and G. Thurston. 2006. Blockade of Dll4 inhibits tumour growth by promoting non-productive angiogenesis. *Nature.* 444:1032–1037. https://doi.org/10.1038/nature05355

Oh, D.S., H. Kim, J.E. Oh, H.E. Jung, Y.S. Lee, J.-H. Park, and H.K. Lee. 2017a. Intratumoral depletion of regulatory T cells using CD25-targeted photodynamic therapy in a mouse melanoma model induces antitumoral immune responses. *Oncotarget.* 8:47440–47453. https://doi.org/10.18632/oncotarget.17663

Oh, D.S., J.E. Oh, H.E. Jung, and H.K. Lee. 2017b. Transient Depletion of CD169+ Cells Contributes to Impaired Early Protection and Effector CD8+ T Cell Recruitment against Mucosal Respiratory Syncytial Virus Infection. *Front. Immunol.* 8:819. https://doi.org/10.3389/fimmu.2017.00819

Okabe, K., S. Kobayashi, T. Yamada, T. Kurihara, I. Tai-Nagara, T. Miyamoto, Y.S. Mukouyama, T.N. Sato, T. Suda, M. Ema, and Y. Kubota. 2014. Neurons limit angiogenesis by titrating VEGF in retina. *Cell.* 159:584–596. https://doi.org/10.1016/j.cell.2014.09.025

Pàez-Ribes, M., E. Allen, J. Hudock, T. Takeda, H. Okuyama, F. Viñals, M. Inoue, G. Bergers, D. Hanahan, and O. Casanovas. 2009. Antiangiogenic therapy elicits malignant progression of tumors to increased local invasion and distant metastasis. *Cancer Cell.* 15:220–231. https://doi.org/10.1016/j.ccr.2009.01.027

Park, J.-S., I.-K. Kim, S. Han, I. Park, C. Kim, J. Bae, S.J. Oh, S. Lee, J.H. Kim, D.-C. Woo, et al. 2016. Normalization of Tumor Vessels by Tie2 Activation and Ang2 Inhibition Enhances Drug Delivery and Produces a Favorable Tumor Microenvironment. *Cancer Cell.* 30:953–967. https://doi.org/10.1016/j.ccell.2016.10.018

Patel, N.S., J.-L. Li, D. Generali, R. Poulsom, D.W. Cranston, and A.L. Harris. 2005. Up-regulation of delta-like 4 ligand in human tumor vasculature and the role of basal expression in endothelial cell function. *Cancer Res.* 65:8690–8697. https://doi.org/10.1158/0008-5472.CAN-05-1208

Phoenix, T.N., D.M. Patmore, S. Boop, N. Boulos, M.O. Jacus, Y.T. Patel, M.F. Roussel, D. Finkelstein, L. Goumnerova, S. Perreault, et al. 2016. Medulloblastoma Genotype Dictates Blood Brain Barrier Phenotype. *Cancer Cell.* 29:508–522. https://doi.org/10.1016/j.ccell.2016.03.002

Reis, M., C.J. Czupalla, N. Ziegler, K. Devraj, J. Zinke, S. Seidel, R. Heck, S. Thom, J. Macas, E. Bockamp, et al. 2012. Endothelial Wnt/β-catenin signaling inhibits glioma angiogenesis and normalizes tumor blood vessels by inducing PDGF-B expression. *J. Exp. Med.* 209:1611–1627. https://doi.org/10.1084/jem.20111580

Ridgway, J., G. Zhang, Y. Wu, S. Stawicki, W.-C. Liang, Y. Chanthery, J. Kowalski, R.J. Watts, C. Callahan, I. Kasman, et al. 2006. Inhibition of Dll4 signalling inhibits tumour growth by deregulating angiogenesis. *Nature.* 444:1083–1087. https://doi.org/10.1038/nature05313

Saharinen, P., L. Eklund, K. Pulkki, P. Bono, and K. Alitalo. 2011. VEGF and angiopoietin signaling in tumor angiogenesis and metastasis. *Trends Mol. Med.* 17:347–362. https://doi.org/10.1016/j.molmed.2011.01.015

Schlecker, E., A. Stojanovic, C. Eisen, C. Quack, C.S. Falk, V. Umansky, and A. Cerwenka. 2012. Tumor-infiltrating monocytic myeloid-derived suppressor cells mediate CCR5-dependent recruitment of regulatory T cells favoring tumor growth. *J. Immunol.* 189:5602–5611. https://doi.org/10.4049/jimmunol.1201018

Scholz, A., P.N. Harter, S. Cremer, B.H. Yalcin, S. Gurnik, M. Yamaji, M. Di Tacchio, K. Sommer, P. Baumgarten, O. Bähr, et al. 2016. Endothelial cell-derived angiopoietin-2 is a therapeutic target in treatment-naive and bevacizumab-resistant glioblastoma. *EMBO Mol. Med.* 8:39–57. https://doi.org/10.15252/emmm.201505505

Scott, A., M.B. Powner, and M. Fruttiger. 2014. Quantification of vascular tortuosity as an early outcome measure in oxygen induced retinopathy (OIR). *Exp. Eye Res.* 120:55–60. https://doi.org/10.1016/j.exer.2013.12.020

Subramanian, A., P. Tamayo, V.K. Mootha, S. Mukherjee, B.L. Ebert, M.A. Gillette, A. Paulovich, S.L. Pomeroy, T.R. Golub, E.S. Lander, and J.P. Mesirov. 2005. Gene set enrichment analysis: a knowledge-based approach for interpreting genome-wide expression profiles. *Proc. Natl. Acad. Sci. USA.* 102:15545–15550. https://doi.org/10.1073/pnas.0506580102

Takano, S. 2012. Glioblastoma angiogenesis: VEGF resistance solutions and new strategies based on molecular mechanisms of tumor vessel formation. *Brain Tumor Pathol.* 29:73–86. https://doi.org/10.1007/s10014-011-0077-6

Van der Veldt, A.A., M. Lubberink, I. Bahce, M. Walraven, M.P. de Boer, H.N. Greuter, N.H. Hendrikse, J. Eriksson, A.D. Windhorst, P.E. Postmus, et al. 2012. Rapid decrease in delivery of chemotherapy to tumors after anti-VEGF therapy: implications for scheduling of anti-angiogenic drugs. *Cancer Cell.* 21:82–91. https://doi.org/10.1016/j.ccr.2011.11.023

Verhaak, R.G., K.A. Hoadley, E. Purdom, V. Wang, Y. Qi, M.D. Wilkerson, C.R. Miller, L. Ding, T. Golub, J.P. Mesirov, et al. Cancer Genome Atlas Research Network. 2010. Integrated genomic analysis identifies clinically relevant subtypes of glioblastoma characterized by abnormalities in PDGFRA, IDH1, EGFR, and NF1. *Cancer Cell.* 17:98–110. https://doi.org/10.1016/j.ccr.2009.12.020

Wang, R., K. Chadalavada, J. Wilshire, U. Kowalik, K.E. Hovinga, A. Geber, B. Fligelman, M. Leversha, C. Brennan, and V. Tabar. 2010. Glioblastoma stem-like cells give rise to tumour endothelium. *Nature.* 468:829–833. https://doi.org/10.1038/nature09624

Wilke, H., K. Muro, E. Van Cutsem, S.-C. Oh, G. Bodoky, Y. Shimada, S. Hironaka, N. Sugimoto, O. Lipatov, T.-Y. Kim, et al. RAINBOW Study Group. 2014. Ramucirumab plus paclitaxel versus placebo plus paclitaxel in patients with previously treated advanced gastric or gastro-oesophageal junction adenocarcinoma (RAINBOW): a double-blind, randomised phase 3 trial. *Lancet Oncol.* 15:1224–1235. https://doi.org/10.1016/S1470-2045(14)70420-6

Yan, H., D.W. Parsons, G. Jin, R. McLendon, B.A. Rasheed, W. Yuan, I. Kos, I. Batinic-Haberle, S. Jones, G.J. Riggins, et al. 2009. IDH1 and IDH2 mutations in gliomas. *N. Engl. J. Med.* 360:765–773. https://doi.org/10.1056/NEJMoa0808710

Yang, H., S. Lee, S. Lee, K. Kim, Y. Yang, J.H. Kim, R.H. Adams, J.M. Wells, S.J. Morrison, G.Y. Koh, and I. Kim. 2013. Sox17 promotes tumor angiogenesis and destabilizes tumor vessels in mice. *J. Clin. Invest.* 123:418–431. https://doi.org/10.1172/JCI64547

Yin, J., Y.T. Oh, J.-Y. Kim, S.S. Kim, E. Choi, T.H. Kim, J.H. Hong, N. Chang, H.J. Cho, J.K. Sa, et al. 2017. Transglutaminase 2 inhibition reverses mesenchymal transdifferentiation of glioma stem cells by regulating C/EBPβ signaling. *Cancer Res.* 77:4973–4984.

Zhou, Y., J. Williams, P.M. Smallwood, and J. Nathans. 2015. Sox7, Sox17, and Sox18 cooperatively regulate vascular development in the mouse retina. *PLoS One.* 10:e0143650. https://doi.org/10.1371/journal.pone.0143650